MINISTRY OF TECHNOLOGY

AERONAUTICAL RESEARCH COUNCIL

CURRENT PAPERS

BEDFORD.

Drag Measurements on a Series of Afterbodies at Transonic Speeds Showing the Effect of Sting Interference

by

A. G. Kurn

LONDON: HER MAJESTY'S STATIONERY OFFICE

1968

NINE SHILLINGS NET

DRAG MEASUREMENTS ON A SERIES OF AFTERBODIES AT TRANSONIC SPEEDS SHOWING THE EFFECT OF STING INTERFERENCE

by

A. G. Kurn

SUMMARY

A number of axi-symmetric afterbodies consisting of the basic profile, a tangent ogive with a fineness ratio of 3.33, and progressively truncated versions of this shape were tested at zero incidence over a Mach number range from 0.8 to 1.3. Measurements were made of the afterbody pressure distribution, the base pressure and the total drag with and without the presence of various rear stings.

In general the drag, in the absence of a sting, was increased by truncating the ogive, but at supersonic speeds small truncations had little effect. The results at a given free stream Mach number show that, for the different stings fitted to each afterbody, there is an approximately linear relationship between afterbody drag and base pressure. Curves are presented whereby the measured total drag of the sting-mounted afterbody model may be corrected to obtain the true total drag in the absence of the sting.

<div align="center">CONTENTS</div>

I   INTRODUCTION

A model supported in a wind tunnel by a sting at the rear must, of necessity, have a bluff base to house the sting. Whether or not this bluff base represents the correct full-scale shape, errors in measured forces are introduced by an incorrect base pressure and the forward influence of the sting. The problem of sting interference and the interpretation of base pressure measurements on bluff based bodies of revolution have received a great deal of attention, both experimentally and theoretically. However, there are so many independent variables that a general solution at both super-sonic and subsonic speeds, and for a variety of body and sting shapes, requires extensive experimental data, so that the scope of any one test must necessarily be severely limited.

The pressure on the base of a body is determined by the state of the external field, the state of the boundary layer at the end of the afterbody, and the rate of mixing in the separated region behind the base. It is, there-fore, dependent on several variables, including Mach number, Reynolds number and the location of transition. To give an indication of the wide variation in base pressure with Reynolds number, a typical curve for a cylindrical body at a supersonic speed is shown in Fig.1. This figure has been taken from Ref.1 which contains also an explanation of the shape of the curve based on the original analysis of Crocco and Lees[2]. It will be seen (Fig.1) that with a well developed turbulent boundary layer on the body there is a gradual decrease in base pressure ratio with increase in Reynolds number. However, at low supersonic Mach numbers the base pressure ratio is high[1], so that although a change in Reynolds number may only alter the base pressure ratio slightly, base drag, being proportional to $(1 - p_B/p_\infty)$ is altered by a much larger factor. This indicates that small-scale model testing at low supersonic speeds, could seriously under-estimate the drag of a full-scale vehicle when base drag is a major item.

Supporting a model by a sting attached to the base may well interfere with the pressure on the base and pressures over the afterbody. A number of supersonic investigations into sting-support interference have focussed attention on sting design giving little or no interference. Such investigations have been made with cylindrical stings, and for convenience the interference has been considered in terms of sting diameter and length. Lee and Summers[3] have shown that at transonic speeds, both for a cylindrical body and for one particular shape of afterbody, a sting of any finite diameter interferes with the base pressure.

At supersonic speeds the critical length* of a sting depends mainly on Mach number, but Whitfield[4] has shown that the Reynolds number also has some effect. At transonic and subsonic speeds disturbances are propagated well upstream so that the critical sting length is probably greater.

This brief survey indicates that wind tunnel experiments on small-scale models supported at the rear by a sting may yield values of the afterbody and base drag which differ significantly from the full-scale values. The transonic investigation described herein has been made on a family of after-bodies at zero incidence attached to an upstream support. The experiment was carried out at a fixed Reynolds number, with a turbulent boundary layer which varied slightly in thickness depending on the Mach number. The aim of the investigation was firstly, to determine the afterbody pressure distribution, the base pressure and the drag of a pointed ogival afterbody which was progressively truncated, leaving a bluff base. Secondly, the effect of a variety of stings mounted behind these bases was investigated.

2 EXPERIMENTAL DETAILS

The investigation was made in the R.A.E. 2 ft × 1.5 ft transonic tunnel at a unit Reynolds number of 2.69 million per foot. The Mach number range covered was from 0.8 to 1.3.

Each model was attached to a strain-gauge balance mounted at the down-stream end of a 1.5 inch diameter support tube (Fig.2). The balance fitted into a compartment in the body so that, except for a small gap to prevent the support interferring mechanically with the balance, the model was continuous with the tube. The support tube, which was located on the longitudinal centre-line of the tunnel, by a mounting upstream in the subsonic contraction, enclosed the electrical leads from the balance and tubes from pressure holes in the model.

2.1 The models

The complete afterbody, representing the rear end of a typical fuselage without a tail-unit, is shown in Fig.2(a). Truncated versions of this shape, finishing at the positions indicated in the figure, represented the basic body shortened to take various sizes of sting support. The position of the balance compartment made it impracticable to manufacture a model reduced in length to the

---

*By definition, changes in sting shape downstream of the critical length have no effect on the base pressure.

cylindrical section of the basic shape; to investigate this case the model shown in Fig.2(b) was tested.

To accommodate the stings, a hole 0.6 in deep was made in the base of each model. This hole was slightly greater in diameter than 0.8 times the base diameter, to provide clearance between base and sting. It was not blanked for the tests without a sting.

2.2   The stings

Details of the stings tested and the models to which they were fitted are listed in Table 1. Each sting was equipped with a short cylindrical spigot which fitted into the hole in the base of the model with a clearance of about 0.030 in. Larger stings were made with the same size spigot and an increase in diameter just behind the base. For smaller stings, short inserts about 0.1 in deep were fitted into the base hole to maintain the clearance gap. To illustrate this change in goemetry with sting size five cases are shown in Fig.3.

All the stings with the exception of two (cases 14 and 23) were tapered from the base. The two exceptions had a cylindrical section from the base before taper commenced. The basic model was also tested with a pointed probe located about 0.030 in behind the afterbody (case 2).

Downstream, the stings were attached to a cone with a 45° vertex angle and a maximum diameter of 2.5 in. Including this cone the stings varied in length from about 14.25 in to 18 in, depending on the position of the base of the model.

2.3   Balance pressure

Throughout the tests the pressure in the balance compartment was recorded. Measurements of drag force have been adjusted to values that would have occurred if this pressure had been equal to free stream static pressure.

2.4   Base pressure

The base pressure, measured either on the model or on the front of a sting (Fig.3), has been used to determine base drag coefficient C_{D_B} defined by $C_{D_B} = - (D/D_M)^2 C_{p_B}$. The total drag, that is the drag measured by the strain-gauge balance when adjusted for the pressure in the balance compartment, has had the base drag subtracted from it to obtain afterbody drag i.e.

$$C_{D_A} = C_D - C_{D_B}.$$

Pressures measured on the front of the sting for case 20 (see Fig.3) indicated that the pressure in the base compartment was fairly uniform. Also, for all the cases with the cylindrical body, the values of afterbody drag coefficient agreed with skin friction estimates to within ±0.005 over the Mach number range. Thus the measurement of a single base pressure to determine base drag was regarded as justified.

2.5 Boundary layer thickness

Pitot pressure traverses through the boundary layer on the support tube, one inch upstream from the model (2.67 calibres from the commencement of the afterbody), at Mach numbers of 0.90 and 1.20, gave the following thickness values in non-dimensional form

M	δ/D_M	δ^*/D_M	θ/D_M
0.90	0.435	0.0765	0.0435
1.20	0.40	0.066	0.037

[δ, the boundary layer thickness, is defined as the distance from the wall at which the local velocity is 0.99 times the free-stream velocity. δ^* and θ are respectively the displacement and the momentum thicknesses.]

These traverses also showed that the velocity distribution followed the one-seventh power law characteristic of a fully developed turbulent boundary layer.

3 RESULTS

3.1 Afterbody pressures

The pressure distributions measured on the basic model alone, Case 1, and with a probe behind it, Case 2, are presented in Fig.4(a), while Figs.4(b) to 4(e) show the effects of shortening the afterbody and including stings at the base.

Referring first to Fig.4(a) it can be seen that a probe behind the basic body has a negligible effect on the afterbody pressure distribution. Moreover, the flow is apparently attached over the whole surface, even though the pressure gradient towards the rear of the model is unfavourable.

Truncating the body such that $D/D_M = 0.283$ (Fig.4(b)) does not noticeably change the pressure distribution in the absence of a sting. When, however, various stings are placed behind this base, the pressure is increased slightly towards the rear of the afterbody.

Shortening the body further to give $D/D_M = 0.7C3$ (Fig.4(c)) increases the afterbody pressures, even for the case of the body alone. In the presence of a sting this effect is magnified and, at subsonic Mach numbers, extends over the entire afterbody. However, at supersonic Mach numbers, the effect is confined to the rear portion of the model. A similar trend is to be observed when $D/D_M = 0.939$ (Fig.4(d)), but in this case the data are less comprehensive since only one afterbody pressure point was available.

Fig.4(e) shows the pressure distribution along the cylindrical afterbody $(D/D_M = 1.0)$ with and without a sting. At subsonic speeds it can be seen, in both cases, that the influence of the base extends upstream and causes a decrease in pressure on the cylinder. At $M = 1.2$, however, this effect has become negligible, and the indications are that the pressure which is uniform along the cylinder decreases abruptly to the base pressure at the trailing edge.

3.2   Base pressures

The base pressure results for the different models, with and without stings, are shown in Fig.5, in which C_{p_B} is plotted against M. To illustrate the effect of variations in the sting geometry consider, as a typical example, the two graphs for $D/D_M = 0.703$. Referring to Table 1 it is apparent that for a given minimum sting diameter (d/D constant), increasing the sting vertex angle (ϕ) increases the base pressure. Similarly when ϕ is constant, the base pressure increases as d/D increases. It is also apparent that this interference effect is quite severe, even with stings of relatively modest diameter and vertex angle.

With a cylindrical afterbody and a cylindrical sting of the same diameter $(D/D_M = 1.0$, Case 22), it can be seen that the measured value of C_{p_B} is positive over the whole Mach number range, whereas it should be zero. This error, which may apply also to Cases 21 and 23, is probably due to misalignment of afterbody and sting.

Fig.6 presents the base pressure measurements taken on the bodies without a sting. As D/D_M increases, θ/D and β decrease, so that C_{p_B} is expected to decrease also. This trend is confirmed by the figure which shows further that the curves of C_{p_B} versus $(D/D_M)^2$ are approximately linear for much of their length.

3.3 Total drag

The total drag measurements on the shortened bodies with and without stings are presented in Figs.7(a) to 7(d)*. The maximum cross-sectional area of the bodies (i.e. a 1.5 in diameter circle) has been used as the reference area on which drag coefficients are based.

For the model with D/D_M = 0.283 (Fig.7(a)), the addition of the stings reduces drag by a small amount only. As the base area increases the effect of the stings on drag becomes more significant (Figs.7(b) and 7(c)). Drag is reduced in all cases except for Case 16 (Fig.7(c)), where, above a Mach number of 1.16 approximately the drag becomes greater than that for the body without a sting. It is shown in section 3.4 that at the higher Mach numbers the afterbody drag remains fairly constant, and it is the greater reduction in base pressure with Mach number when the stings are present (Fig.5) which mainly contributes to the drag increase in Case 16. This reduction in base pressure also accounts for the continued rise in drag coefficient for the sting cases, apparent in Fig.7(b) for example, when the drag coefficient has become constant for the case without a sting.

Of the four stings tested with the cylindrical model, three (Cases 21, 22 and 23) were of the same diameter as the base. The total drag results for these cases (Fig.7(d)) are considered to be in error, for the reason given in section 3.2 above. Even so, the total drag and base pressure measurements taken with these stings were self-consistent in that the afterbody drag, calculated by subtraction, agreed with the theoretical skin friction curve (Fig.7(d)) to within ±0.005 in C_D.

3.4 The relationship between base pressure and afterbody drag C_{D_A}

Figs.8(a) to 8(d) relate afterbody drag to base pressure**, when base pressure is changed by altering sting geometry. Fig.8(c), particularly, confirms the discovery by Mc Donald and Hughes[5] that, as the sting geometry is changed, the drag of a given afterbody at a given subsonic Mach number is a

---

*The dip in the curves at a Mach number of about 1.20 is probably due to a temperature gradient across the strain gauge balance, incurred by an increase in power necessary to maintain tunnel flow conditions. Dotted curves have been added to give what is thought to be more accurate drag distributions.

**The base pressures for Case 3 (Fig.8(b)) were not measured. Estimated values were obtained by extrapolating the curves of Fig.4(b).

linear function of base pressure. Further, it would seem that this linear relationship applies also at supersonic Mach numbers above 1.10, with the change in afterbody drag with base pressure becoming quite small at the higher Mach numbers (1.20 and 1.30). Below the critical Mach number of about 0.96 the curves of Fig.8(c) are parallel, which suggests that the slope $(\delta C_{D_A}/\delta C_{p_B})$ of these curves might apply at Mach numbers lower than 0.8.

Fig.8(d) shows that for the afterbody with the largest diameter base there is no apparent change in afterbody drag with base pressure and no appreciable change with Mach number.

The effect on drag and base pressure of altering base geometry was investigated with the afterbody having the largest base and no sting present. The modified base shape (Fig.8(d): Case 15(a)) increased total drag slightly. Fig.8(d) shows that the measured base pressures are raised (giving a reduction in base drag), and there is an increase in the derived afterbody drag. It may be that for this case a single pressure hole is insufficient to determine base drag.

3.5   The total and component drag coefficients without a sting

Fig.9(a) - (c) shows the total and component drag coefficients for the bodies without stings, plotted against Mach number. In these curves the drag of the cylindrical afterbody has been adjusted, by adding a skin friction term, such that its length corresponds to that of the cylindrical position of the ogival afterbodies.

For each configuration Fig.9(a) shows that C_D is practically constant at subsonic Mach numbers (M < 0.95), and at supersonic Mach numbers (M > 1.05), but increases rapidly as M increases from 0.95 to 1.05. Moreover, this change in drag at transonic speeds is only slightly dependent on D/D_M.

Fig.9(b) shows that, as the pointed ogive is progressively truncated, the afterbody drag coefficient (C_{D_A}) first increases and then decreases. This trend, which is particularly noticeable at subsonic speeds, reflects the afterbody pressure distribution (Fig.4), the static pressure being greater than free-stream pressure towards the rear of the afterbody, and less than free-stream static pressure further upstream. The corresponding curves for the base drag coefficient (C_{D_B}) shown in Fig.9(c) call for no special comment.

The results of Fig.9 have been cross-plotted in Fig.10(a) - (c) to show
the variation in drag as the basic body is shortened and the base area increased.
Experimental errors in the total drag and base pressure measurements give a
scatter to the afterbody drag results which increases with base area (Fig.10(b)).
The dotted curve, largely based on skin friction estimates, gives a more accurate
indication of afterbody drag for the larger base areas. It is shown (Fig.10(a))
that, for the subsonic Mach numbers, the total drag coefficient (C_D) is a
minimum for the pointed ogive and increases monotonically as the afterbody is
shortened. At supersonic Mach numbers, however, C_D changes very little with
small reductions in afterbody length, and there is even an indication that the
minimum C_D occurs when the body is truncated slightly as suggested by the
collected data published by Hoerner[5]. Fig.10(a) also shows that the body may be
shortened without increasing C_D by more than about 0.005, providing the ratio
base area/body area is kept below 0.2 at subsonic Mach numbers and 0.4 at
supersonic Mach numbers.

3.6 Corrections to the drag of a sting-mounted body

Frequently the true total drag of an afterbody and base (without a sting)
is required, to correct the measured drag and base pressure of a shortened model
supported in a wind tunnel by a sting at the rear. Figs.11, 12 and 13 present
corrections whereby this may be achieved. The corrections due to the sting
and to shortening the afterbody are treated separately.

If the shortened afterbody is not cylindrical, Fig.11 gives the increment
$(\Delta C_{D_{STING}})$ to be added to the measured drag coefficient (C_{D_M}) to obtain the true
drag coefficient of the shortened model without a sting. If, on the other hand,
the shortened afterbody is cylindrical, the measured base drag coefficient for
the model with sting present is simply replaced by the base drag coefficient for
the model alone shown in Fig.12. In this event it may be noted that there are
no restrictions on sting geometry.

Having eliminated the effects of the sting, the increment in drag coefficient
$(\Delta C_{D_{BODY}})$ incurred simply by shortening the body is taken from Fig.13. Hence the
true drag coefficient for a pointed afterbody model, represented by a sting
mounted model with a shortened afterbody, is determined by the expression
$C_D = C_{D_M} + \Delta C_{D_{STING}} - \Delta C_{D_{BODY}}$. The corrections of Figs.11, 12 and 13, are, of
course, strictly applicable only when the state of the boundary layer conforms
with the conditions given in section 2.5, so it may be assumed that θ/L_M is the
only significant parameter.

Other workers, when comparing afterbodies of different shapes, have brought to light some interesting information. McDonald and Hughes[6], in correlating drag data for circular arc, parabolic and conical afterbodies, from a large number of experiments at high subsonic speeds, found that when the three shapes had identical afterbody angles at the base (β) and identical base diameter ratios (D/D_M) the afterbody drag coefficients were approximately the same, and the base pressure coefficients were approximately the same for the circular arc and the parabola. Moreover calculations based on the work of Reid and Hastings[7] show that when $M = 2.0$, $D/D_M = 0.58$ and $\beta = 10°$, C_{D_B} is the same for both a conical and a parabolic afterbody. It would seem therefore that the drag effects due to sting interference (Fig.11) may perhaps be applied to body shapes that differ slightly from the one tested without incurring too great an error in drag, except possibly in the transonic region. The requirements for a different body shape would be, of course, that D/D_M and β conform with that of the basic afterbody as given in Fig.14.

4   CONCLUSIONS

A tangent-ogival afterbody ending at a point with a fineness ratio of 3.33 and progressively truncated versions of this shape have been tested at zero incidence. The main conclusions drawn from the experiment, which included an investigation into sting interference, are summarised thus.

A   Afterbody pressures (with and without stings)

1   At subsonic speeds, in the absence of a sting, shortening the afterbody has only a small effect on the afterbody pressures. However, a sting behind the base gives rise to an appreciable increase in pressure over the entire afterbody, except when D/D_M is small.

2   At supersonic speeds the afterbody pressures are increased both by truncating the body alone and by adding a sting, but this increase in pressure extends upstream of the base for a short distance only.

B   Base pressures and afterbody drag (with and without stings)

3   In general the presence of a sting increases the basic pressure coefficient.

4   For the bodies without a sting the base pressure coefficient decreases, in an approximately linear manner, as the ratio base area/maximum area increases.

5   For a given afterbody and a given Mach number (less than 0.98 or greater than 1.10), a linear relationship exists between the base pressure coefficient and the afterbody drag coefficient as the sting geometry is varied. At Mach numbers greater than 1.10 the afterbody drag coefficient is rather insensitive to changes in base pressure coefficient.

C   Total drag (without a sting)

6   The complete ogival afterbody (ending at a point) has less total drag at subsonic Mach numbers than any of the truncated versions. However, at supersonic Mach numbers, a shortened afterbody with a small base area appears to have the minimum drag, although the drag for the complete afterbody is only very slightly larger.

7   Providing the base area is less than 0.2 times the body area at subsonic speeds, or 0.4 times the body area at supersonic speeds, the total drag coefficient does not exceed the minimum value by more than 0.005.

8   For each configuration the total drag coefficient (C_D) is approximately constant at Mach numbers less than 0.95 and greater than 1.05. In the transonic range C_D increases abruptly with Mach number, the increment being practically independent of base area ratio.

As the effects of varying boundary layer conditions were not investigated these conclusions must be considered applicable only when the state of the approach boundary layer conforms to that of the experiment.

Table 1

Sting-body configurations

Case No.	Body		Sting		
	D/D_M	$\beta°$	d/D	$\phi°$	Parallel length -calibres (D_M)
1	0	17.1	Body alone		
2			0	2.29	0
3	0.283	14.6	Body alone		
4			0.8	0	-
5			0.8	2.29	0
6			0.5	2.29	0
7	0.703	9.6	Body alone		
8			0.8	0	-
9			0.8	1.145	0
10			0.8	2.29	0
11			0.8	3.435	0
12			0.65	2.29	0
13			0.5	2.29	0
14			0.895	2.85	1
15 and 15a*	0.939	4.4	Body alone		
16			0.8	0	-
17			0.8	2.29	0
18			0.5	2.29	0
19	1.00	0	Body alone		
20			0.8	2.29	0
21			1.0	2.29	0
22			1.0	0	-
23			1.0	2.29	2

*Case 15a - with insert for Case 18 positioned in base hole.

SYMBOLS

C_D	total drag coefficient, based on the maximum cross-sectional area of the body
C_{D_A}	afterbody drag coefficient, based on the maximum cross-sectional area of the body
C_{D_B}	base drag coefficient, based on the maximum cross-sectional area of the body
C_p	pressure coefficient
C_{p_B}	base pressure coefficient
d	diameter of sting at the base
D	base diameter
D_M	maximum body diameter ($= 1$ calibre)
M	free-stream Mach number
p_B	pressure on the base
p_β	pressure on the afterbody immediately upstream of the base
p_∞	free-stream static pressure
x	distance downstream from commencement of afterbody, i.e. where body diameter starts to decrease
β	afterbody angle at the base
δ	boundary layer thickness measured 2.67 calibres upstream from the commencement of the afterbody
δ^*	boundary layer displacement thickness
θ	boundary layer momentum thickness
ϕ	sting vertex semi-angle
$\Delta C_{D_{BODY}}$	the increase in drag coefficient due to shortening the afterbody
$\Delta C_{D_{STING}}$	the decrease in drag coefficient due to positioning a sting at the base of the shortened afterbody

REFERENCES

No.	Author	Title, etc.
1	R.C. Hastings	A note on the interpretation of base pressure measurements in supersonic flows. A.R.C. C.P. 409, June 1958
2	L. Crocco L. Lees	A mixing theory for the interaction between dissipative flows and nearly-isentropic streams. Journal of the Aeronautical Sciences Vol.19, No.10 1952
3	G. Lee J.L. Summers	Effects of sting-support interference on the drag of an ogive-cylinder body with and without a boattail at 0.6 to 1.4 Mach number. NACA RM A57 I09 December 1957
4	J.D. Whitfield	Critical discussion of experiments on support interference at supersonic speeds. Agard Report 300. AEDC-TN-58-30 August 1958
5	S.F. Hoener	Fluid Dynamic Drag (1965 Edition)
6	H. McDonald P.F. Hughes	A correlation of high subsonic afterbody drag in the presence of a propulsive jet or support sting. Journal of Aircraft Vol.2, No.3 May-June 1965
7	J. Reid R.C. Hastings	Experiments on the axi-symmetric flow over afterbodies and bases at M = 2.0. R.A.E. Rept Aero 2628, October 1959, A.R.C.21707
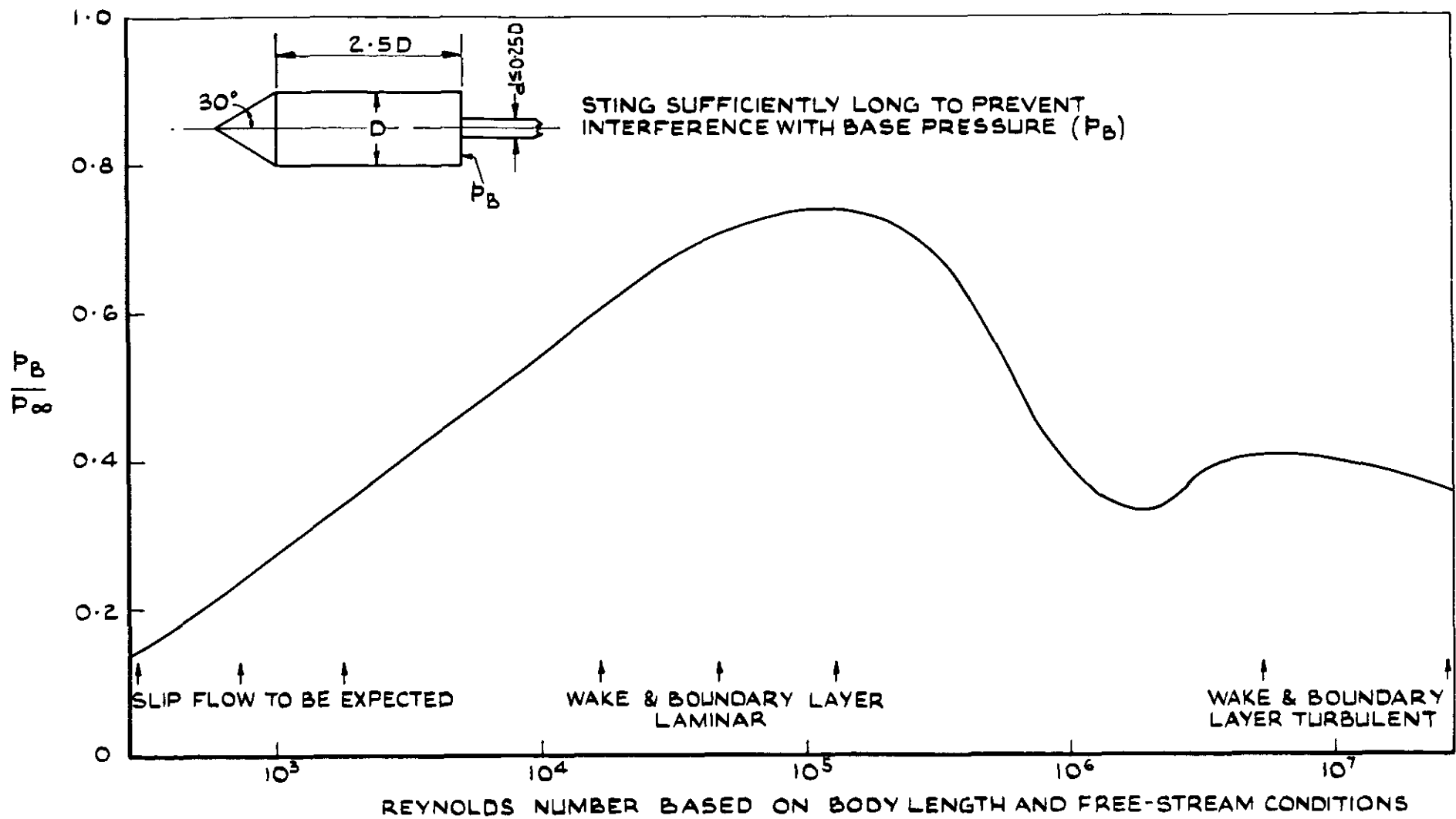
FIG. 1 THE EFFECT OF REYNOLDS NUMBER ON THE BASE PRESSURE OF A CONE –CYLINDER AT M=2·9 APPROX

PRESSURE HOLES

WIND DIRECTION

$0.75 D_M$ | $1.25 D_M$ | $1.75 D_M$ | $2.25 D_M$ | $2.75 D_M$

RADIUS = $11.36 D_M$

$\beta = 17.1°$

$\beta = 14.6°$

$\beta = 9.6°$

$\beta = 4.4°$

$\frac{D}{D_M} = 0.703$

$\frac{D}{D_M} = 0.939$

$\frac{D}{D_M} = 0.283$

$0.5 D_M$

$1.5 D_M$

$2.5 D_M$

$D_M = 1.50"$

OGIVAL SECTION

CYLINDRICAL SECTION

$3.33 D_M (= 5.00")$

$2 D_M (= 3.00")$

BASES OF SHORTENED BODIES

FIG. 2 (a) OGIVAL BODY

$0.25 D_M$ $0.75 D_M$ $1.25 D_M$

PRESSURE HOLES

BALANCE COMPARTMENT

SUPPORT TUBE

D

$D_M = 1.50"$

STRAIN-GAUGE BALANCE

$3.83 D_M (= 5.75")$

FIG. 2 (b) CYLINDRICAL BODY

FIG. 2   DETAILS OF THE AFTERBODIES AND SUPPORT TUBE
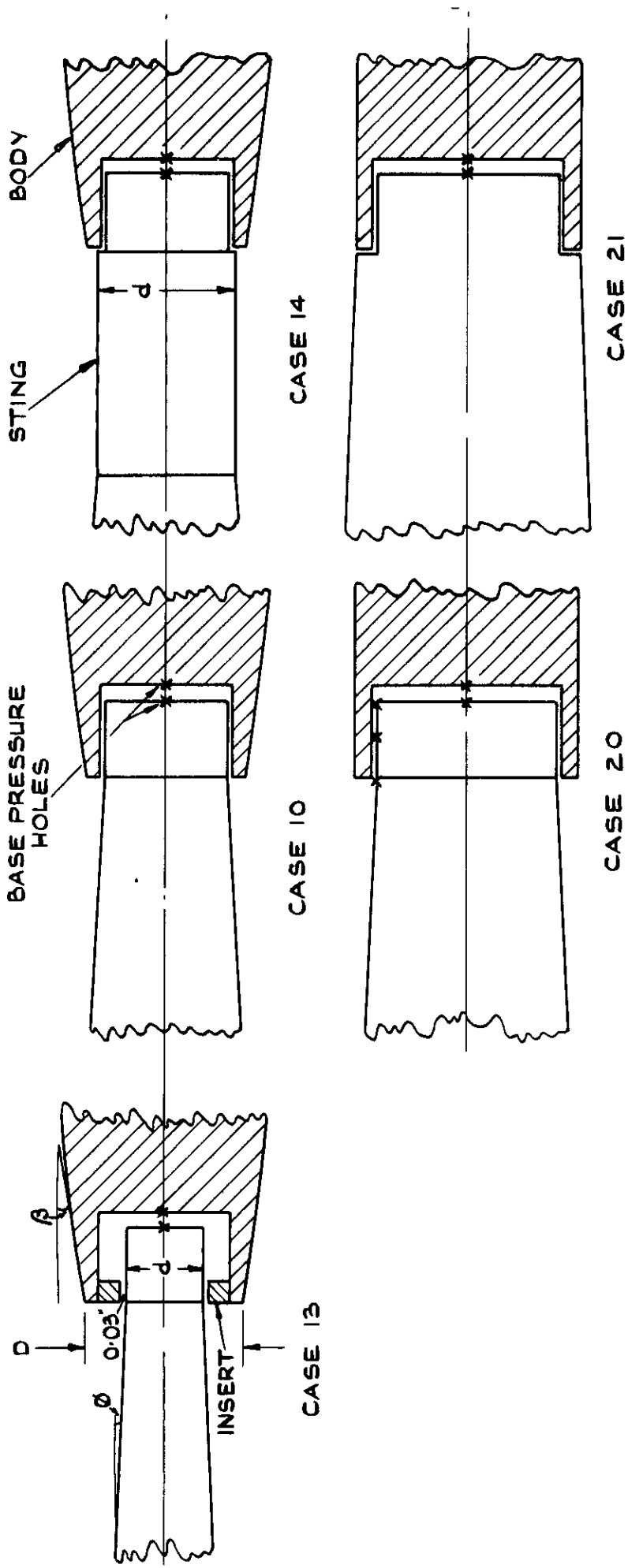
FIG. 3   EXAMPLES OF VARIOUS STING AND BASE CONFIGURATIONS
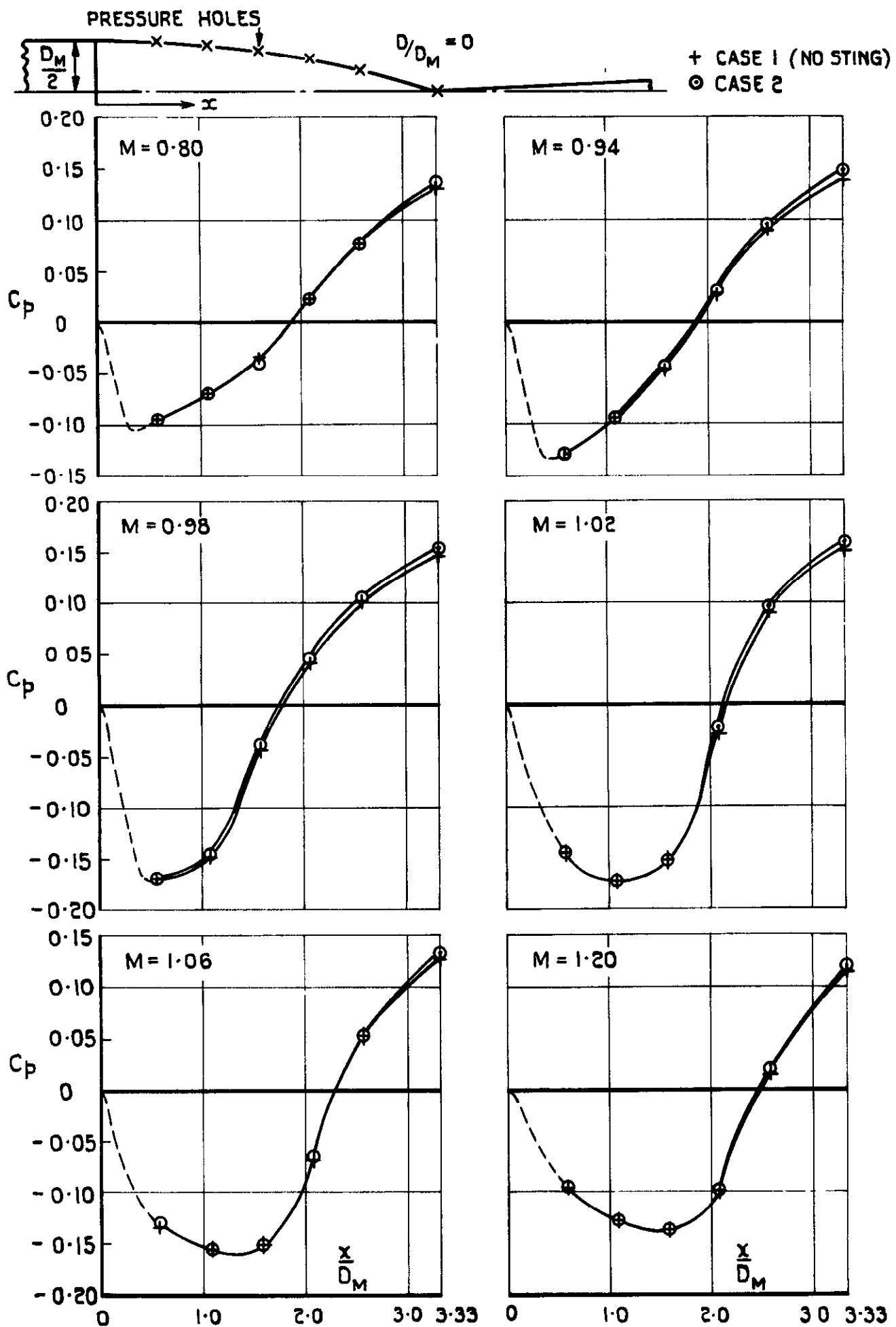
FIG.4(a) THE AFTERBODY PRESSURE DISTRIBUTION $D/D_M = 0$
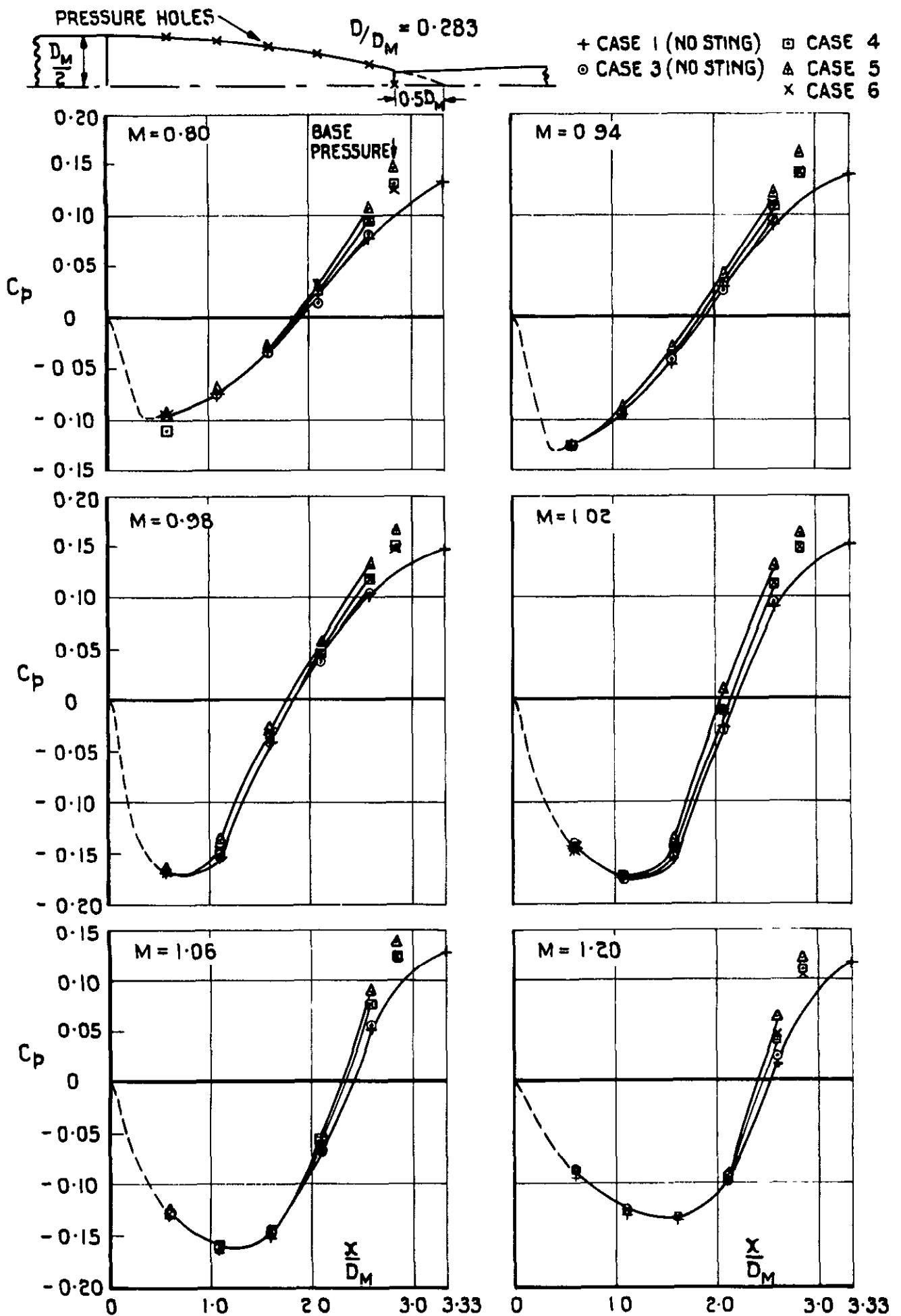
FIG. 4 (b) THE AFTERBODY PRESSURE DISTRIBUTION D/D$_M$=0.283
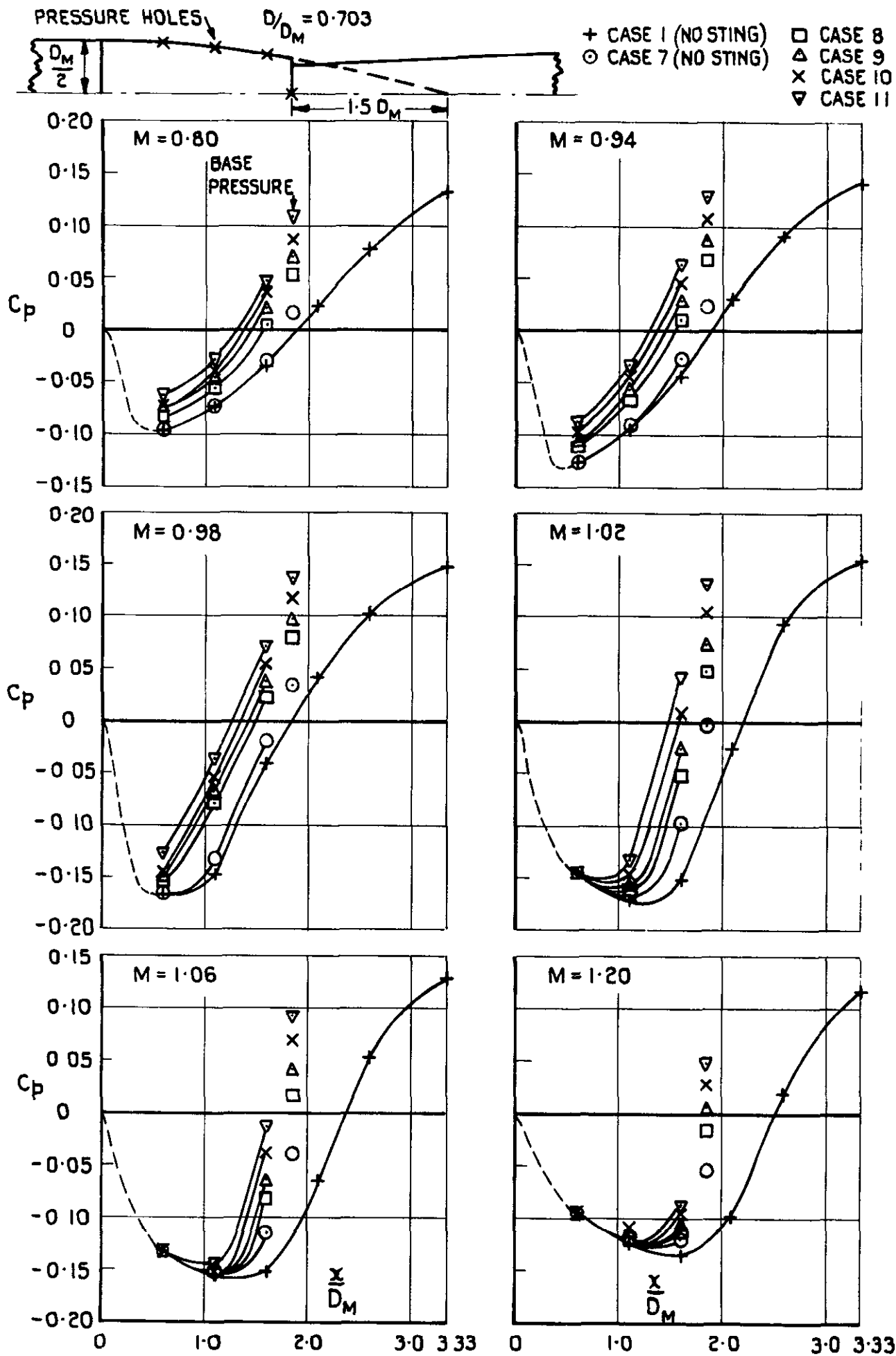
FIG. 4(c) THE AFTERBODY PRESSURE DISTRIBUTION $D/D_M = 0.703$
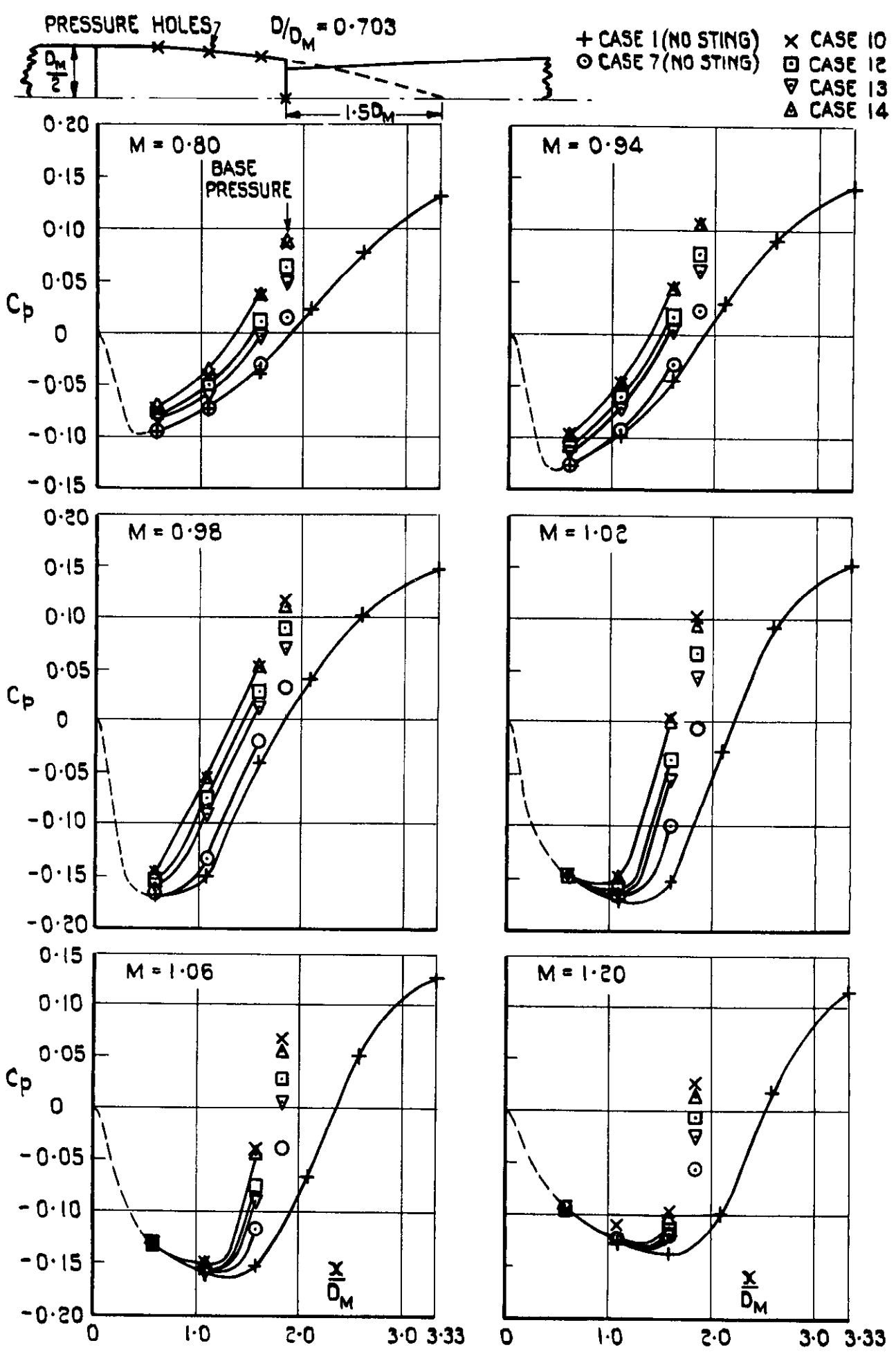
FIG. 4(c) (CONCLD) THE AFTERBODY PRESSURE DISTRIBUTION $D/D_M = 0.703$
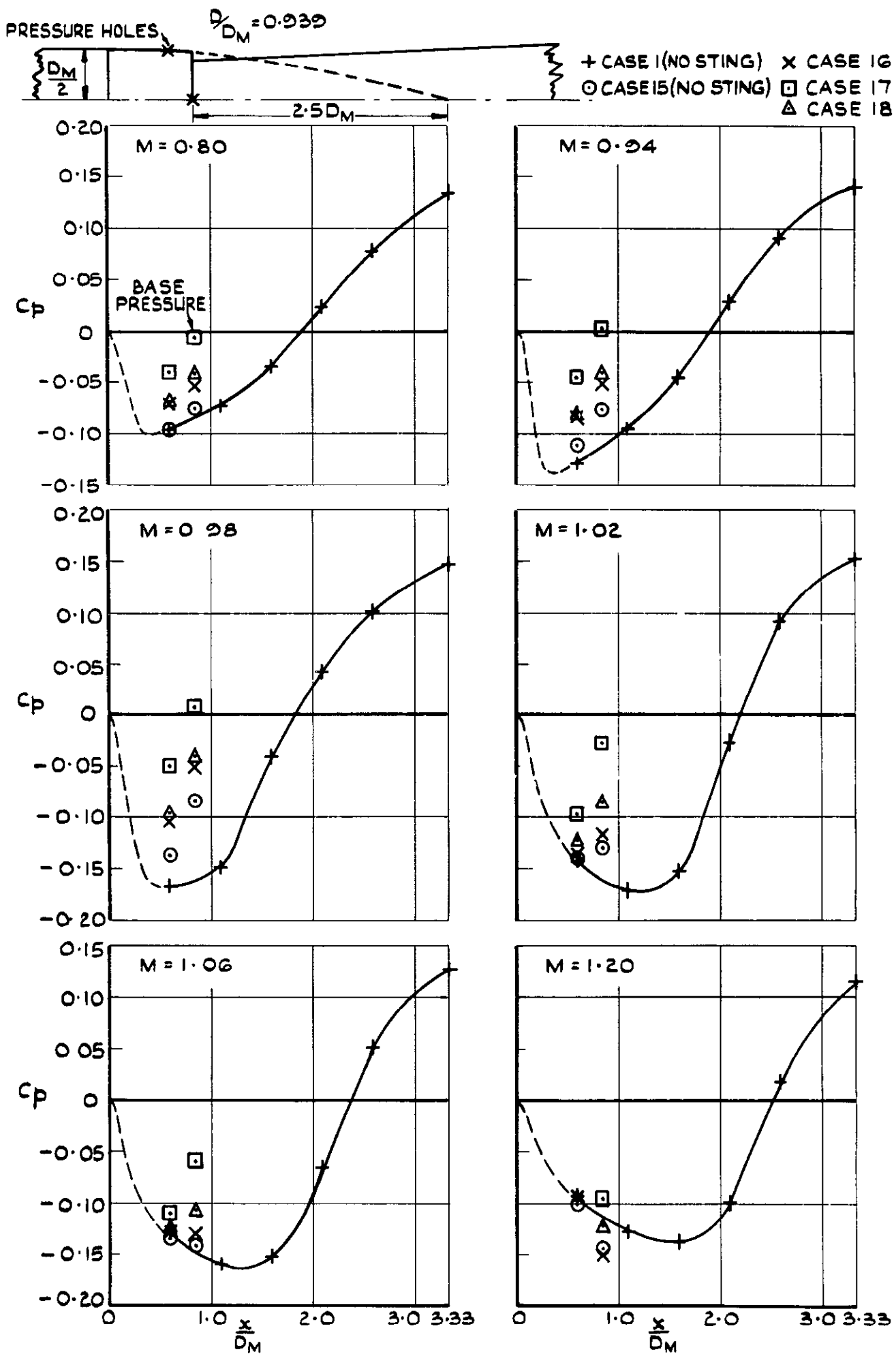
FIG. 4 (d) THE AFTERBODY PRESSURE DISTRIBUTION $D/D_M = 0.939$
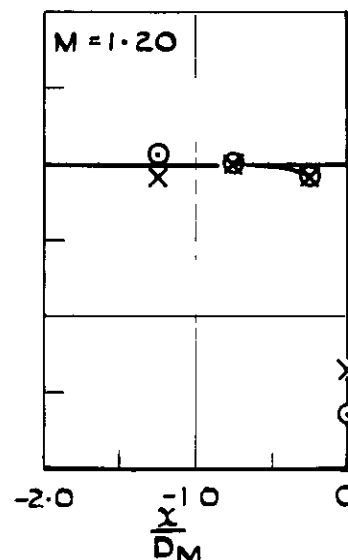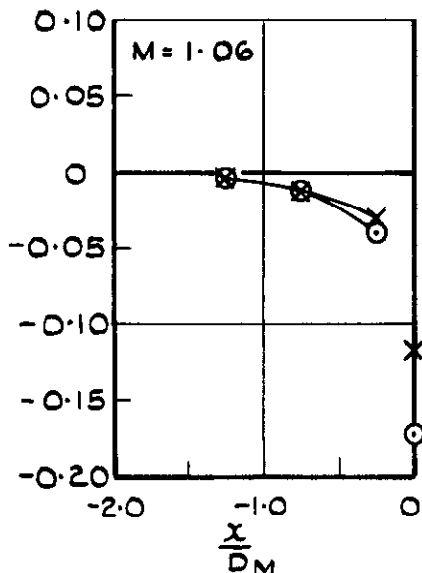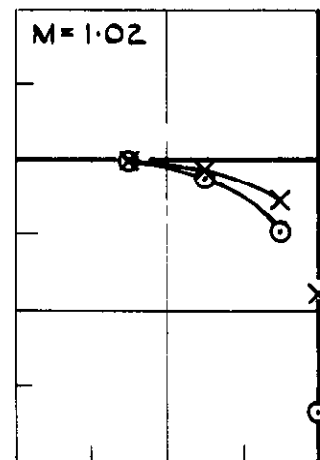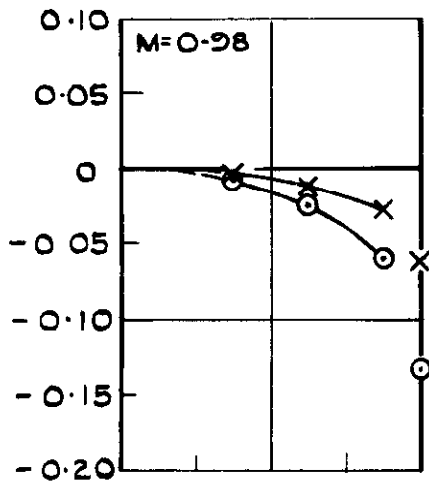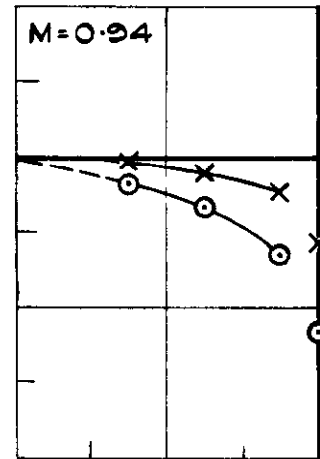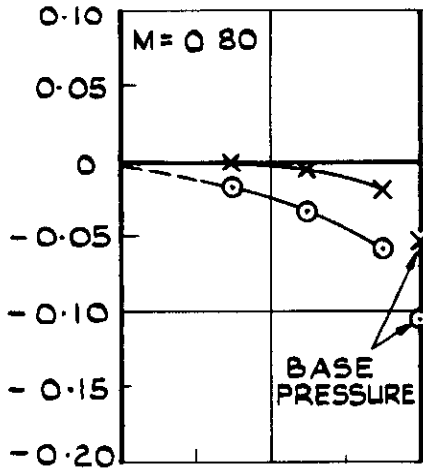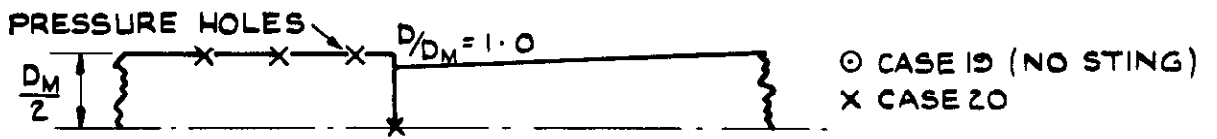
FIG 4 (e) THE AFTERBODY PRESSURE DISTRIBUTION $D/D_M = 1.0$
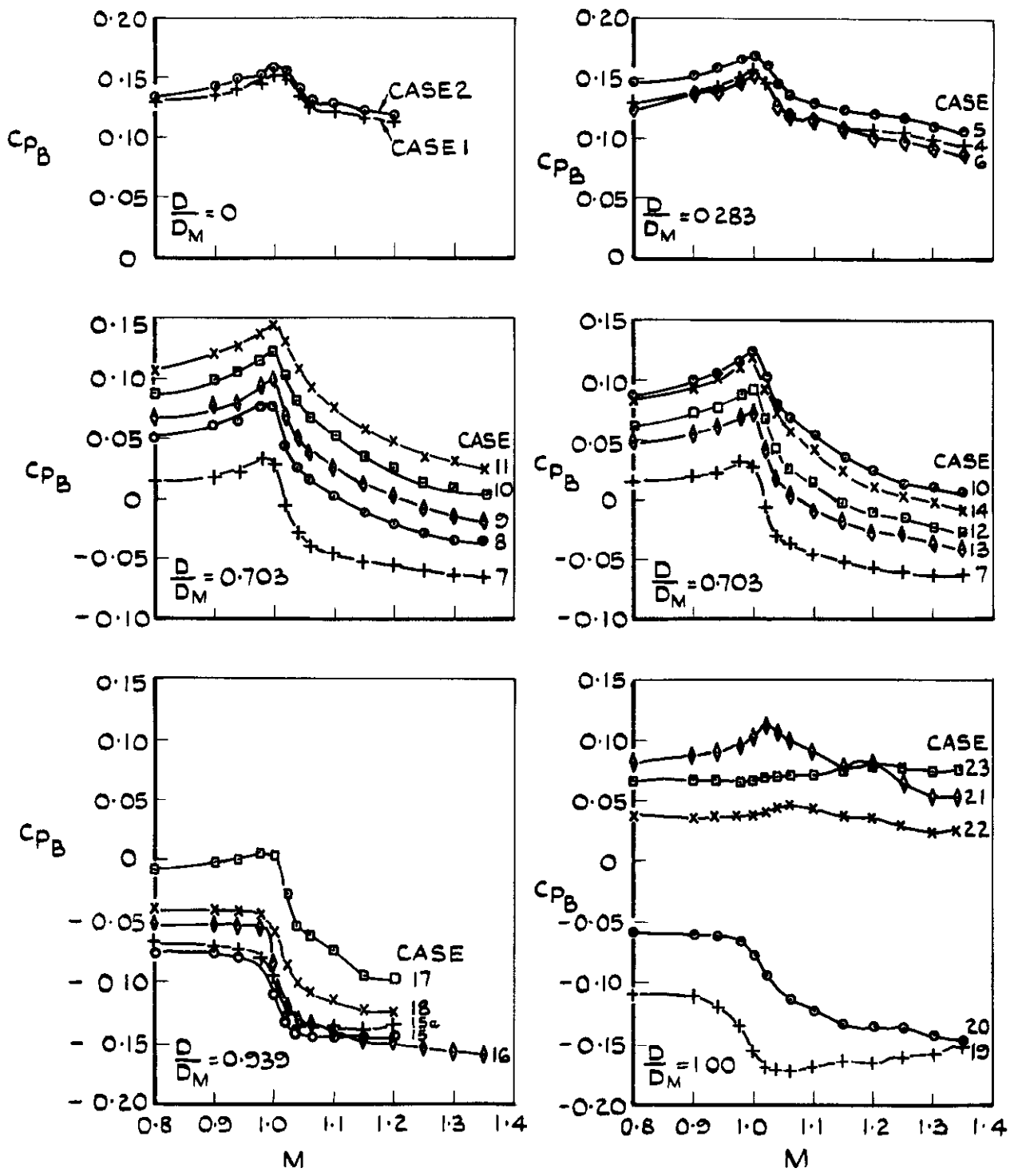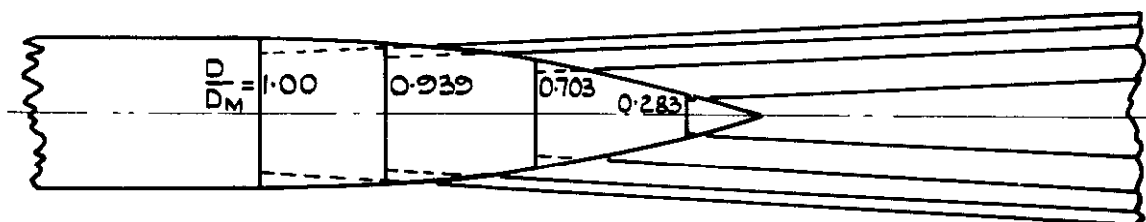
FIG. 5   VARIATION OF BASE PRESSURES WITH
STING GEOMETRY AND MACH NUMBER
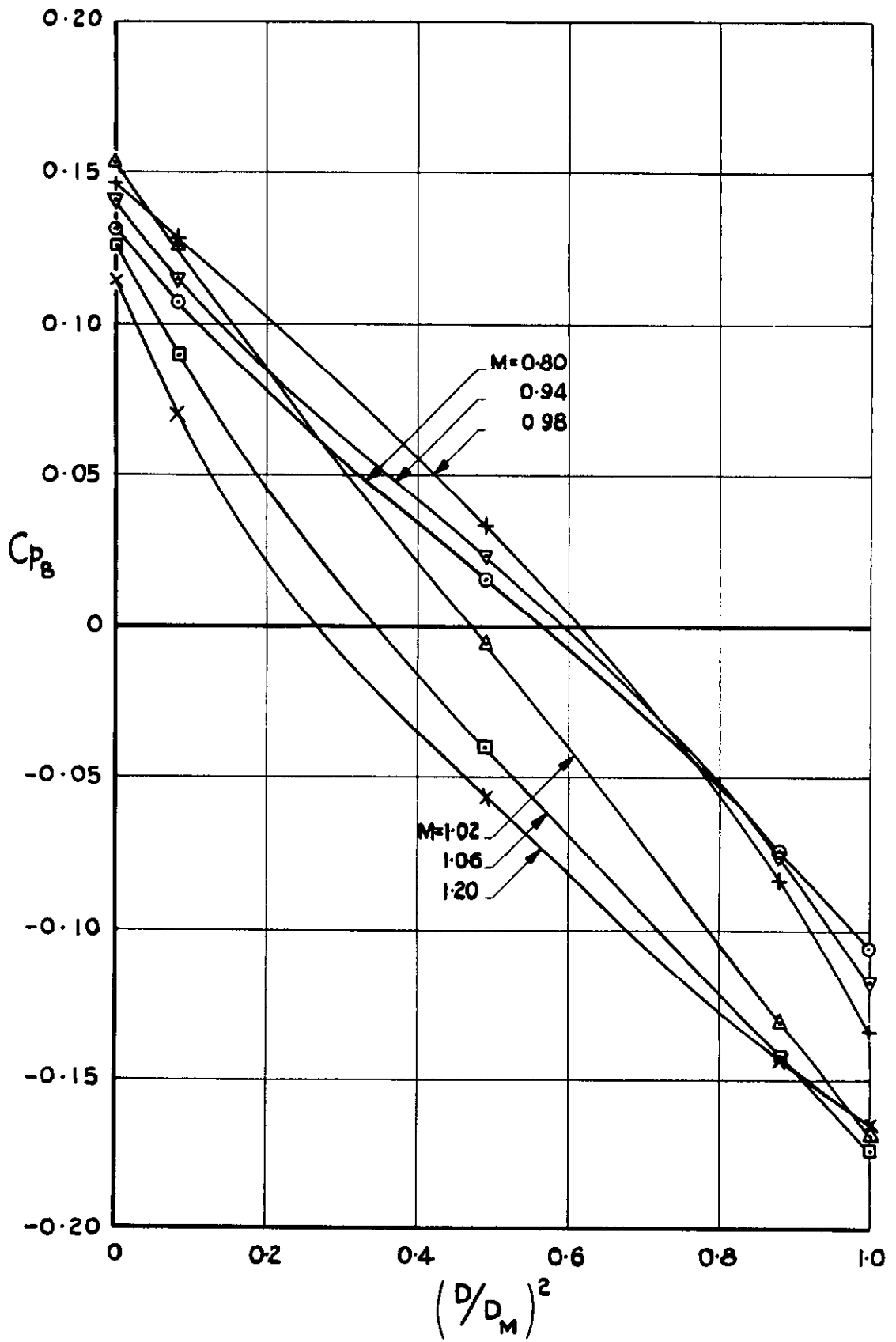
FIG. 6 VARIATION OF BASE PRESSURE WITH
BASE AREA (NO STING)
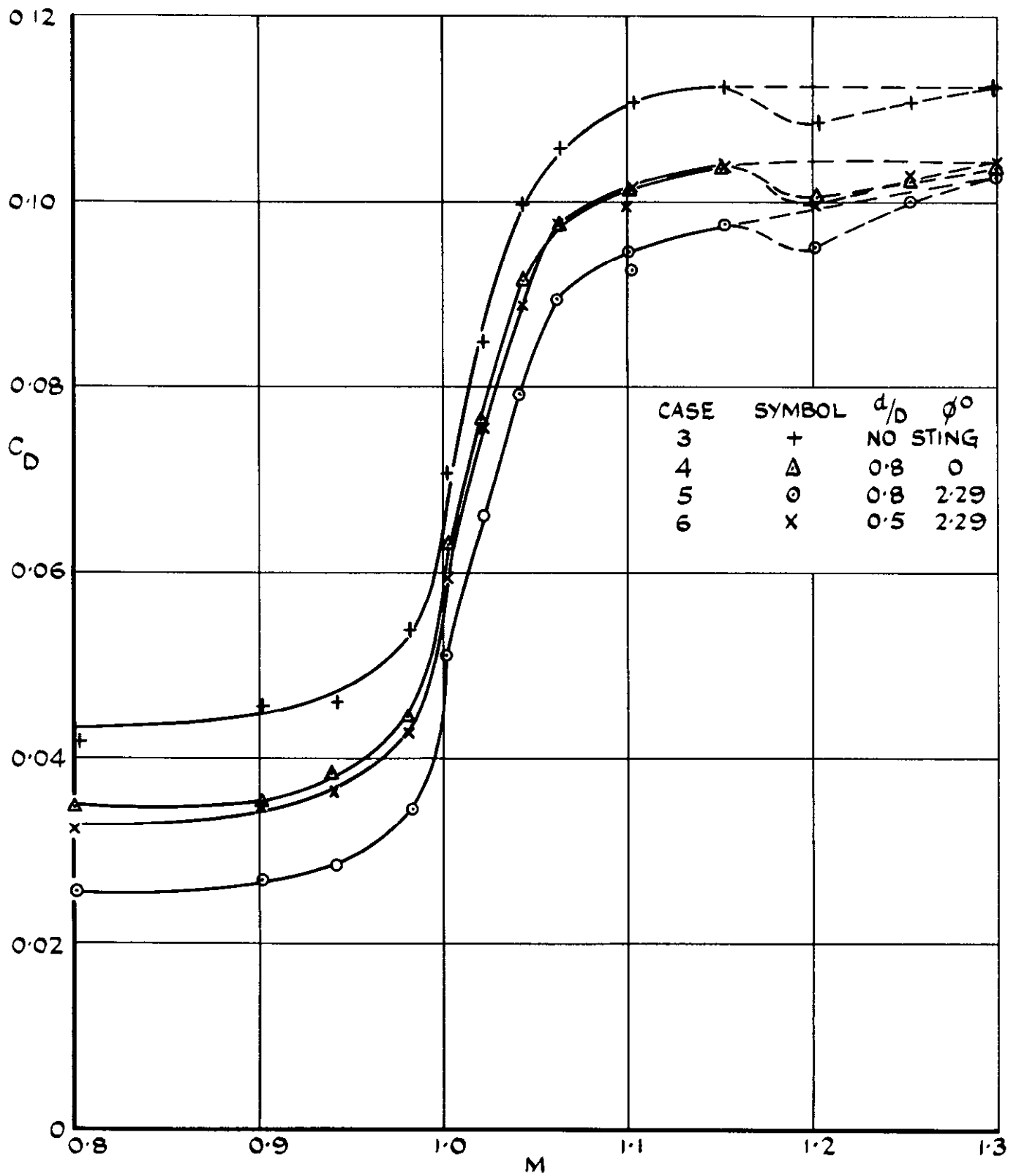
FIG. 7(a) VARIATION OF TOTAL DRAG WITH
STING GEOMETRY AND MACH NUMBER. $D/D_M = 0.283$, $\beta = 14.6°$
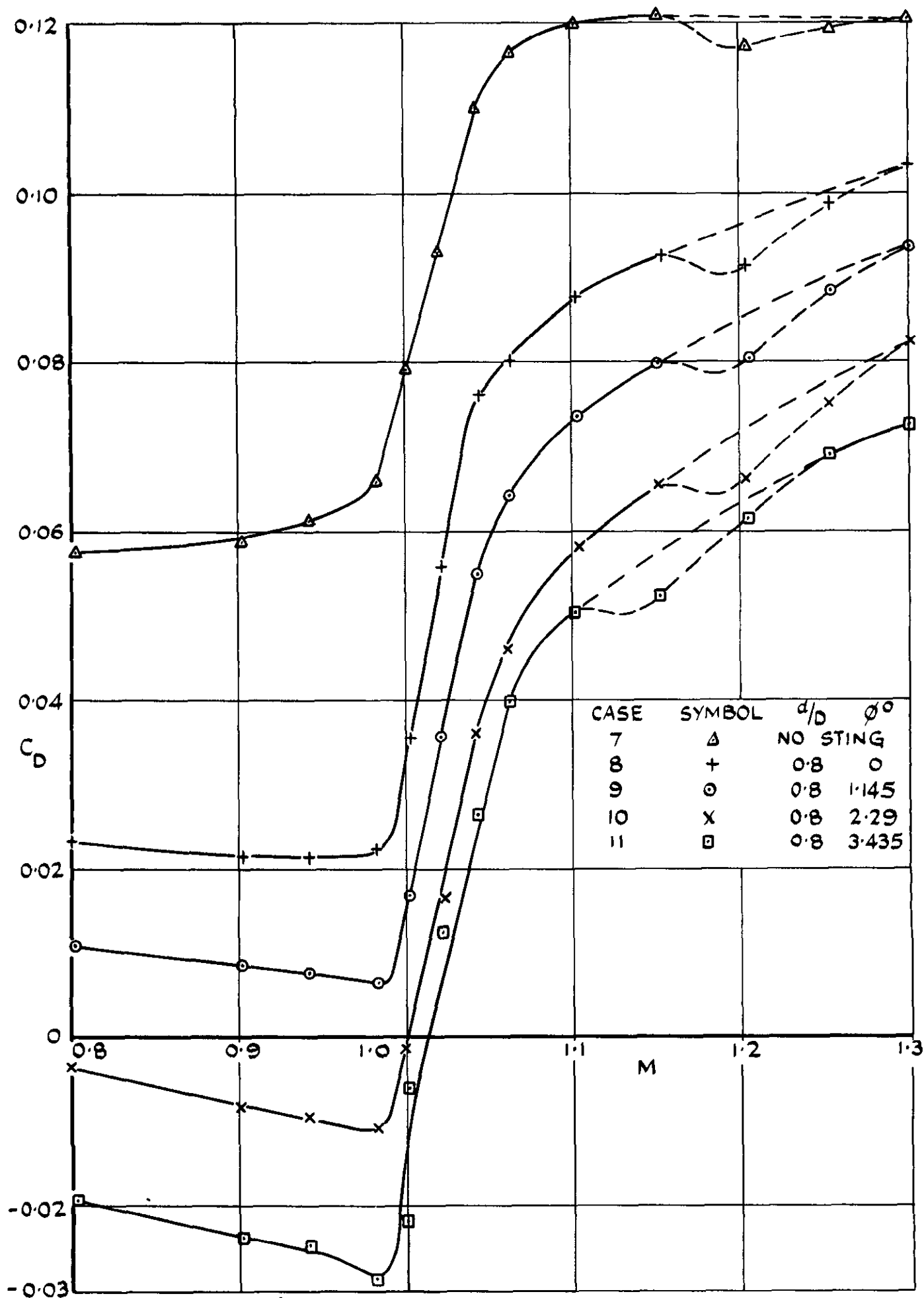
FIG.7 (b) VARIATION OF TOTAL DRAG WITH
STING GEOMETRY AND MACH NUMBER $D_l/D_M = 0.703$ $\beta = 9.6°$
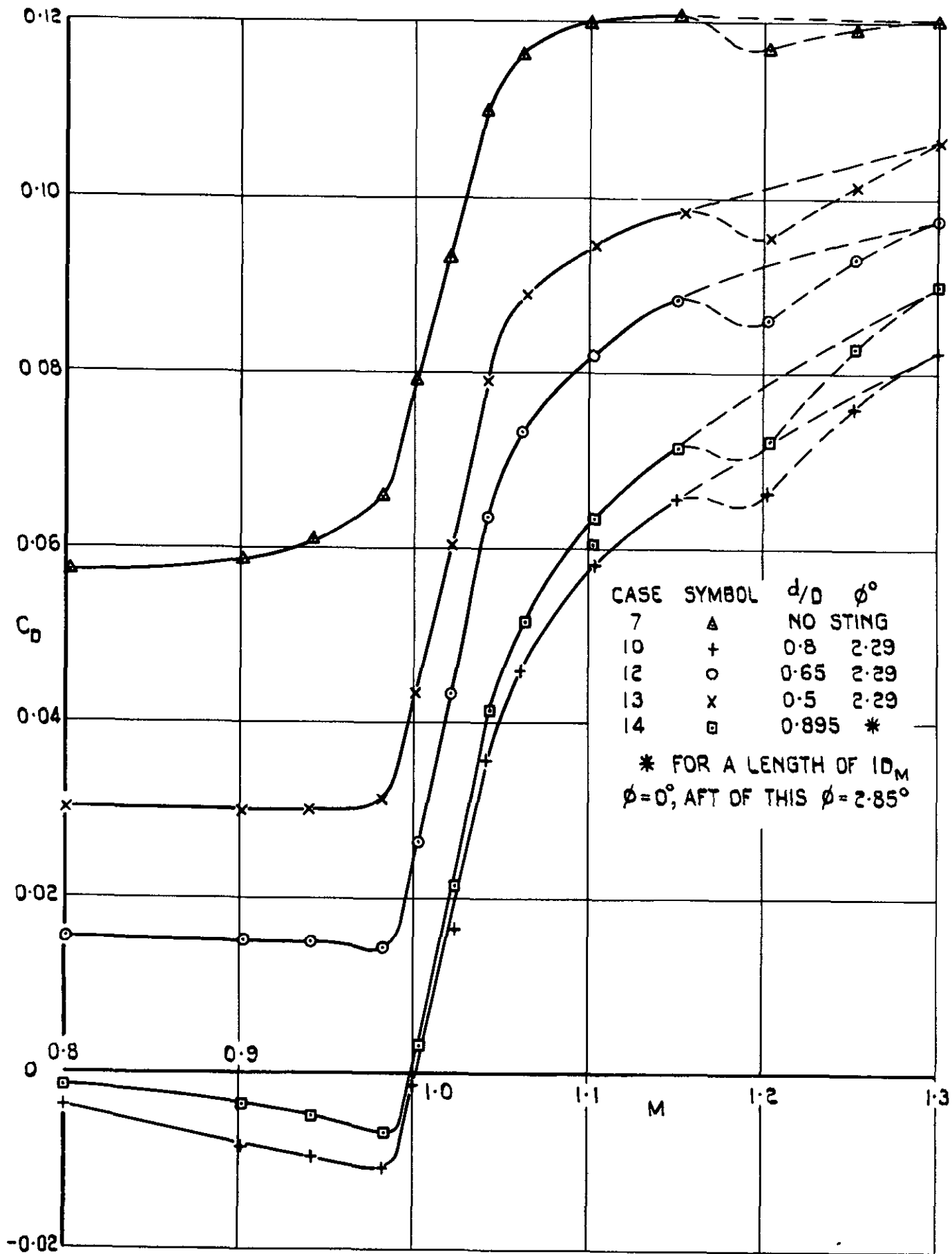
FIG. 7 (b) (CONCLD) VARIATION OF TOTAL DRAG WITH STING GEOMETRY AND MACH NUMBER $D/D_M = 0.703$, $\beta = 9.6°$

CASE	SYMBOL	d/D	ø°
15	x	NO STING	
16	o	0·8	0
17	□	0·8	2·29
18	+	0·5	2·29
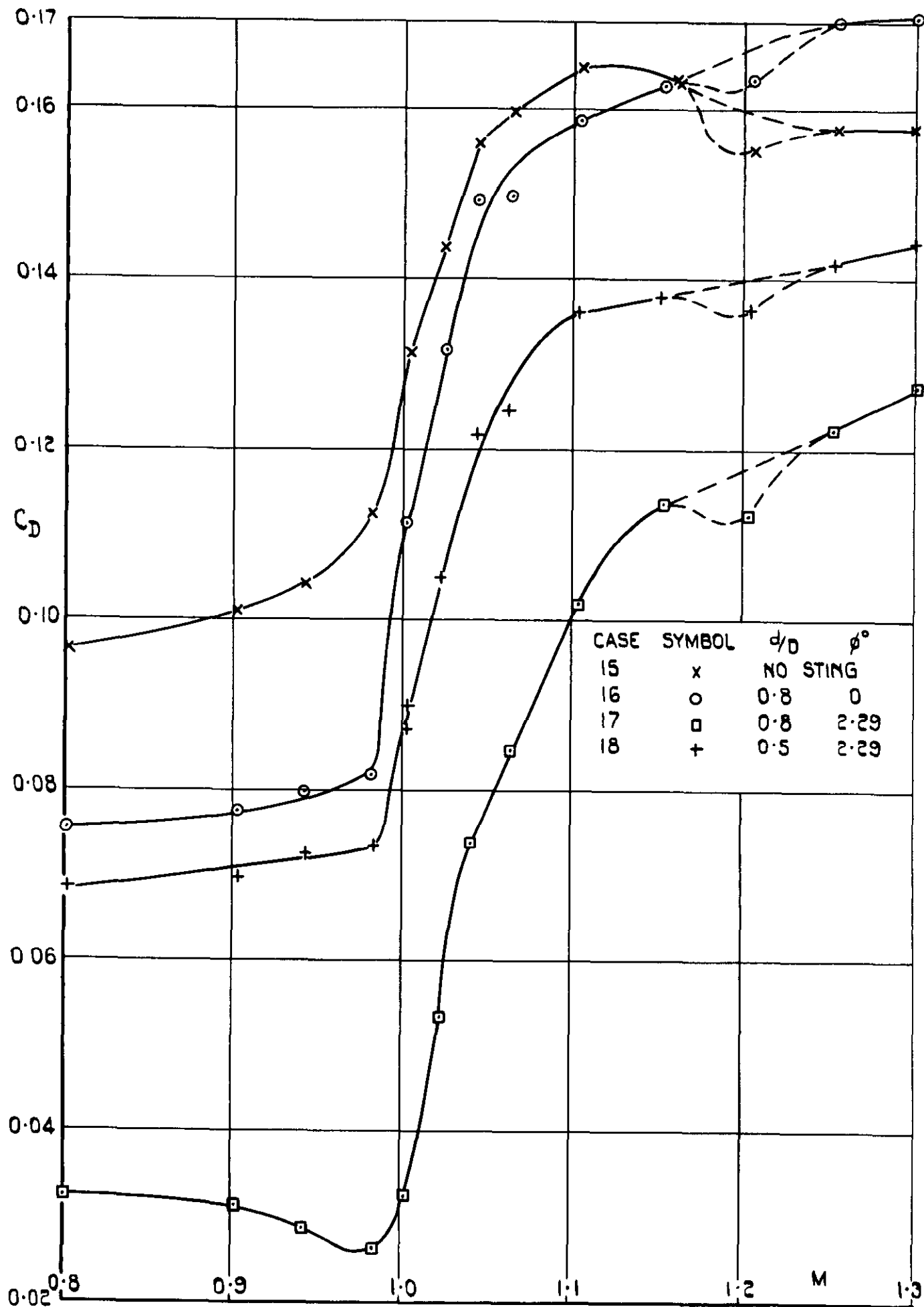
FIG. 7 (c) VARIATION OF TOTAL DRAG WITH STING GEOMETRY AND MACH NUMBER $D/D_M = 0.939, \beta = 4.4°$
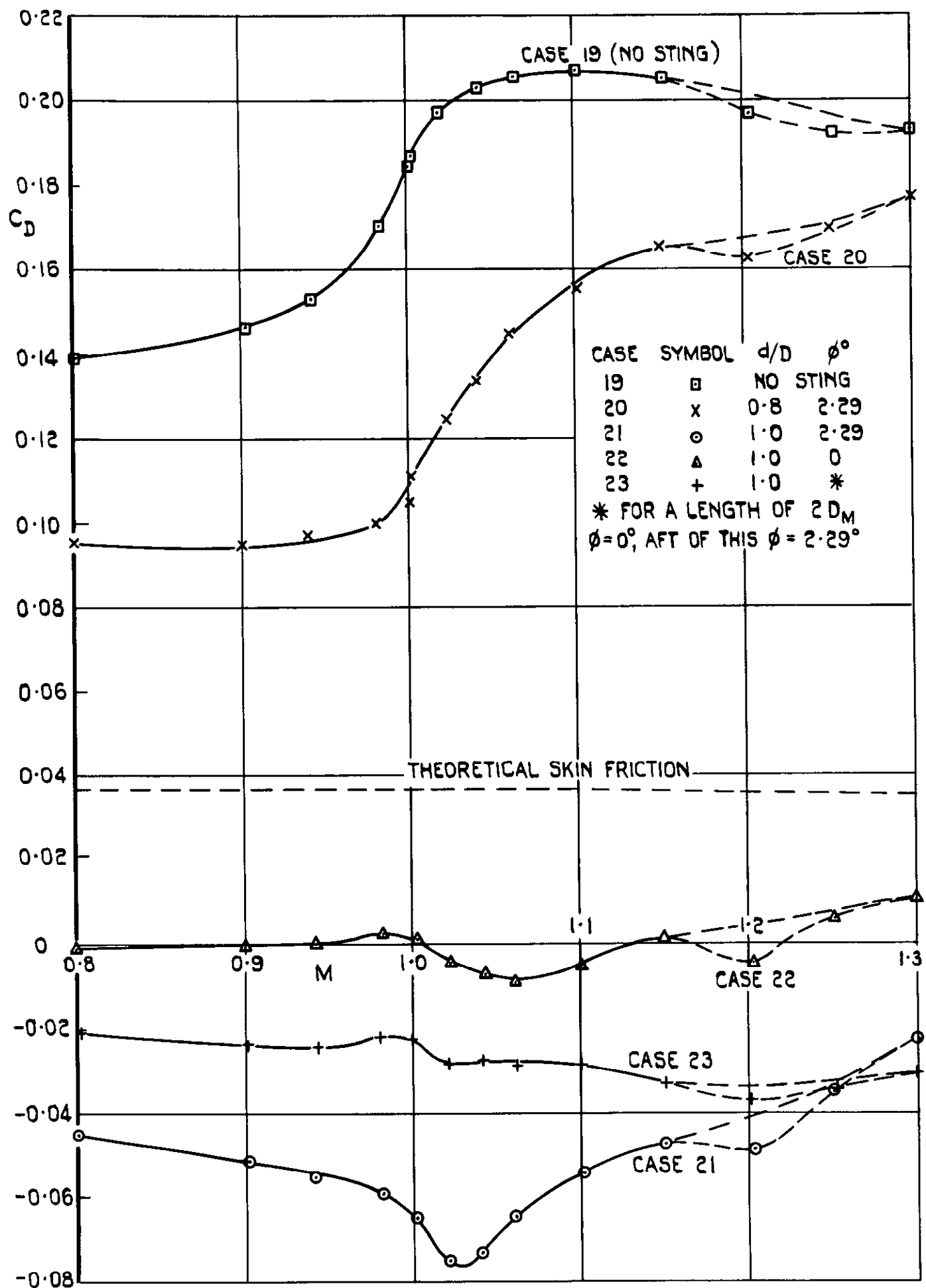
FIG. 7 (d) VARIATION OF TOTAL DRAG WITH
STING GEOMETRY AND MACH NUMBER D/D_M=1·00: β=0°

FIG. 8(a) $D/D_M = O$ $\beta = 17 \cdot 1^{\circ}$
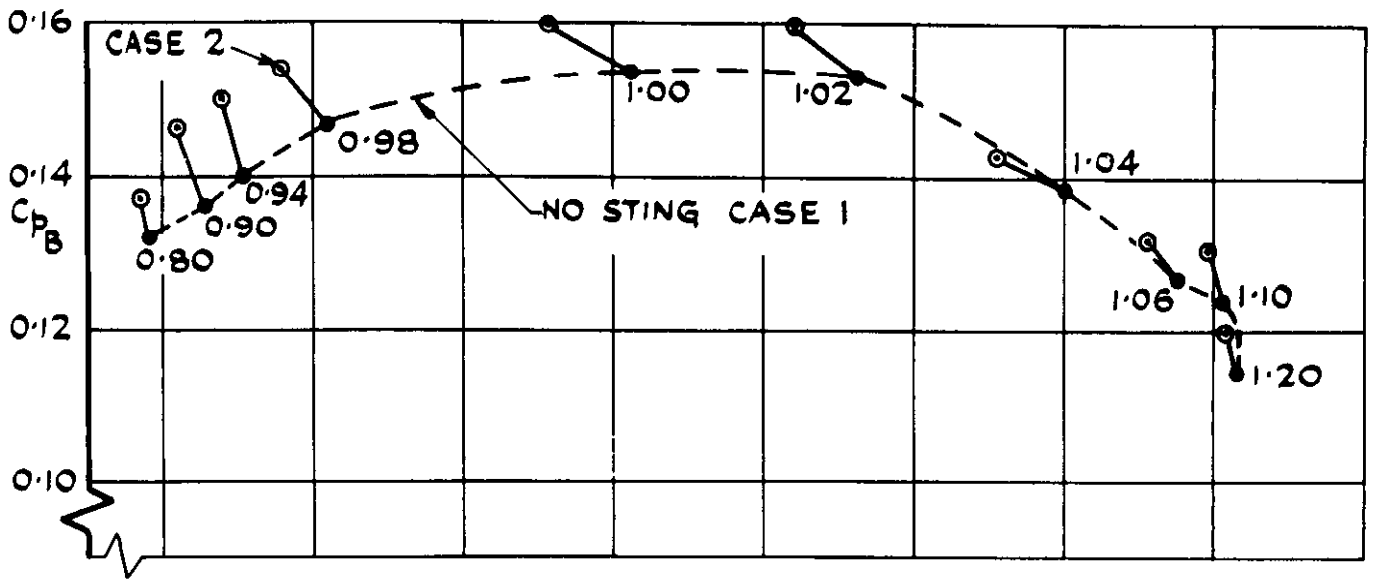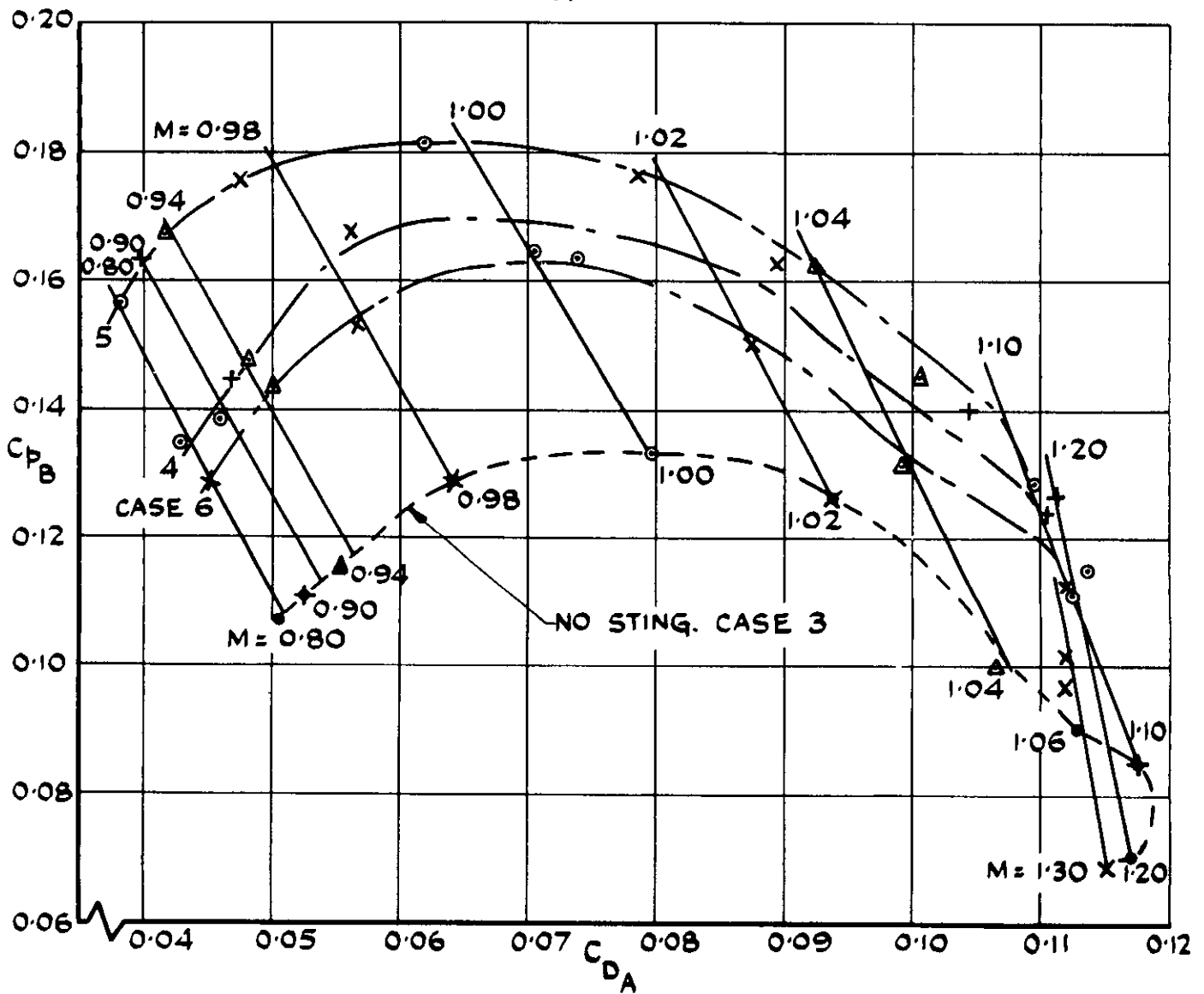
FIG. 8 (b) $D/D_M = O \cdot 283$, $\beta = 14 \cdot 6^{\circ}$

FIG. 8   VARIATION OF AFTERBODY DRAG WITH
BASE PRESSURE AND MACH NUMBER
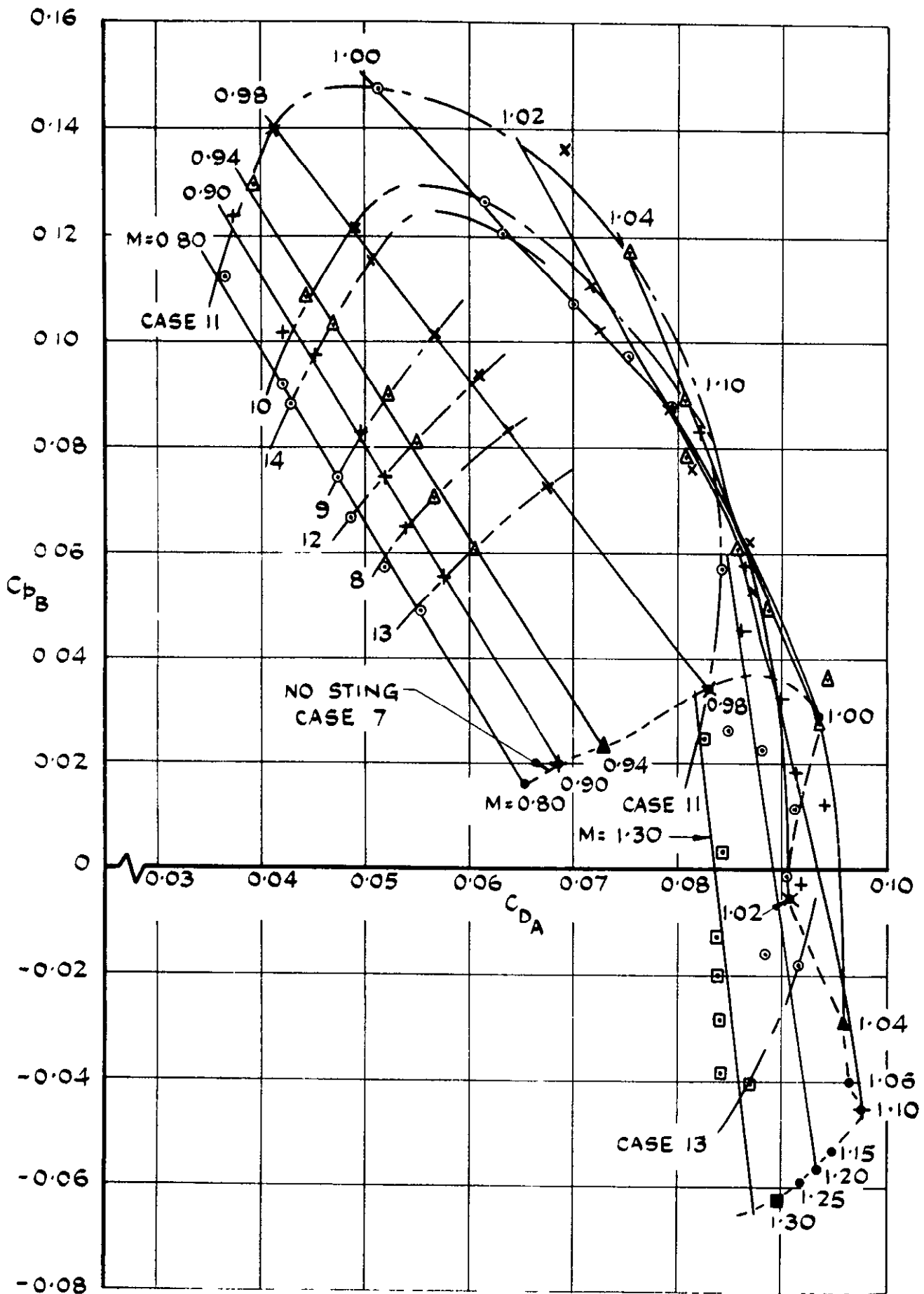
FIG· 8 (c)   VARIATION OF AFTERBODY DRAG WITH BASE PRESSURE AND MACH NUMBER $D/D_M = 0·7C3$, $\beta = 9·6°$

BASE GEOMETRY 'A'
(CASE 15)

BASE GEOMETRY 'B'
(CASE 15a)
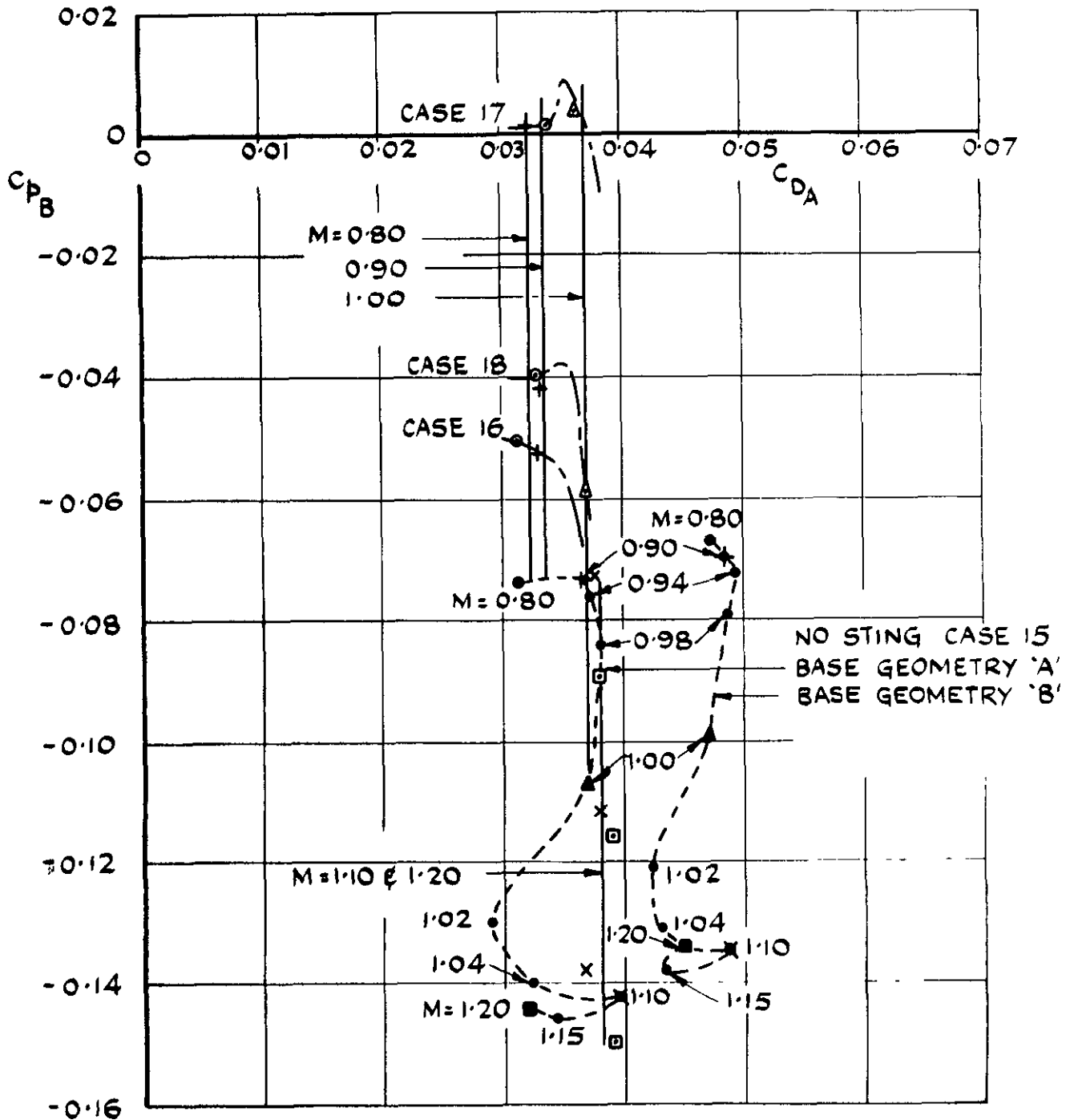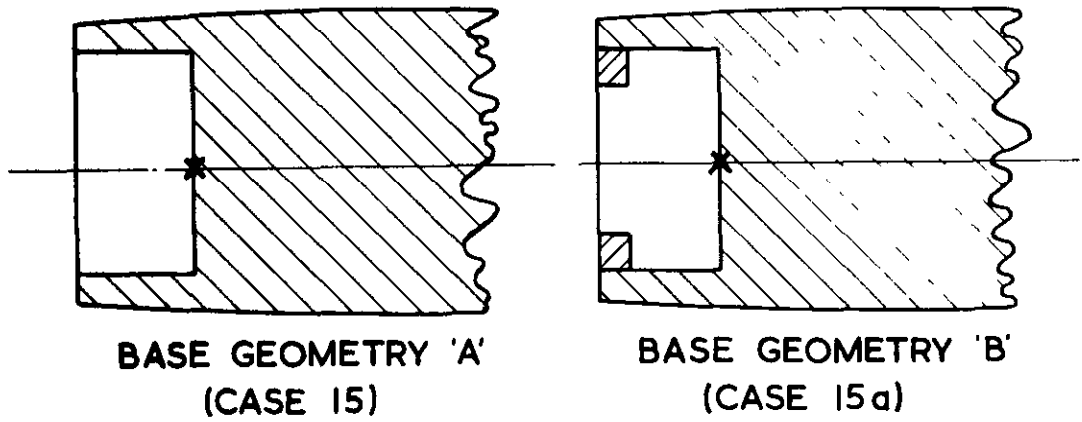
FIG.8 (d) VARIATION OF AFTERBODY DRAG WITH
BASE PRESSURE AND MACH NUMBER $D/D_M = 0.939$, $\beta = 4.4°$
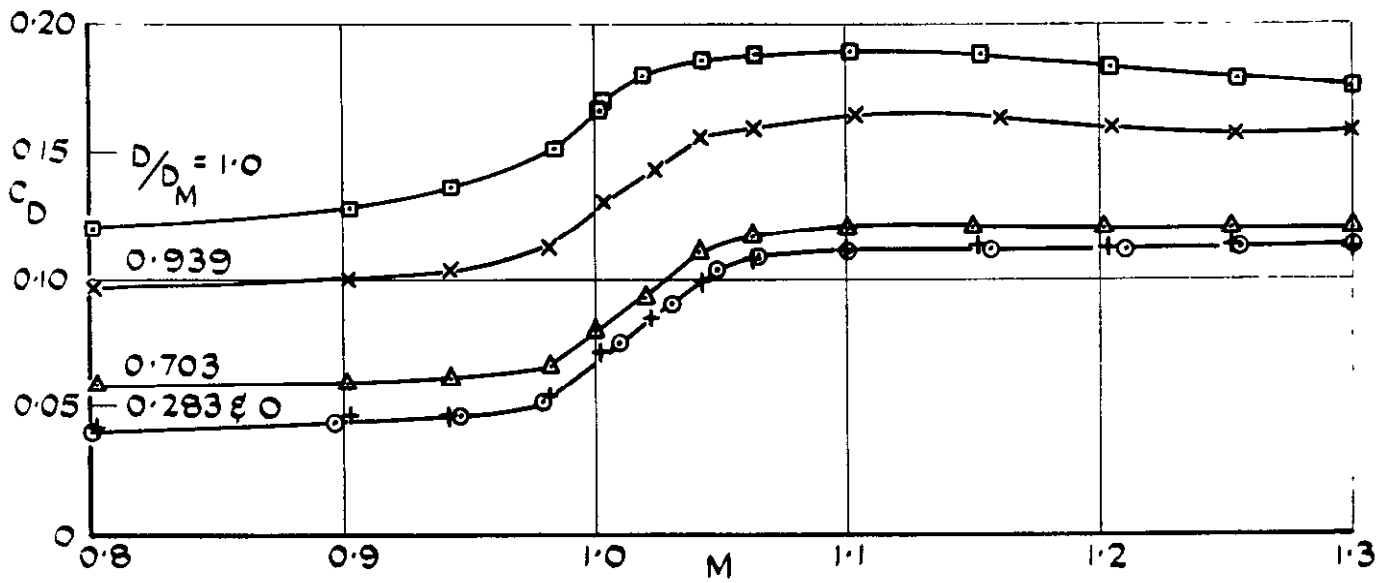
FIG. 9(a) TOTAL DRAG. COEFFICIENT
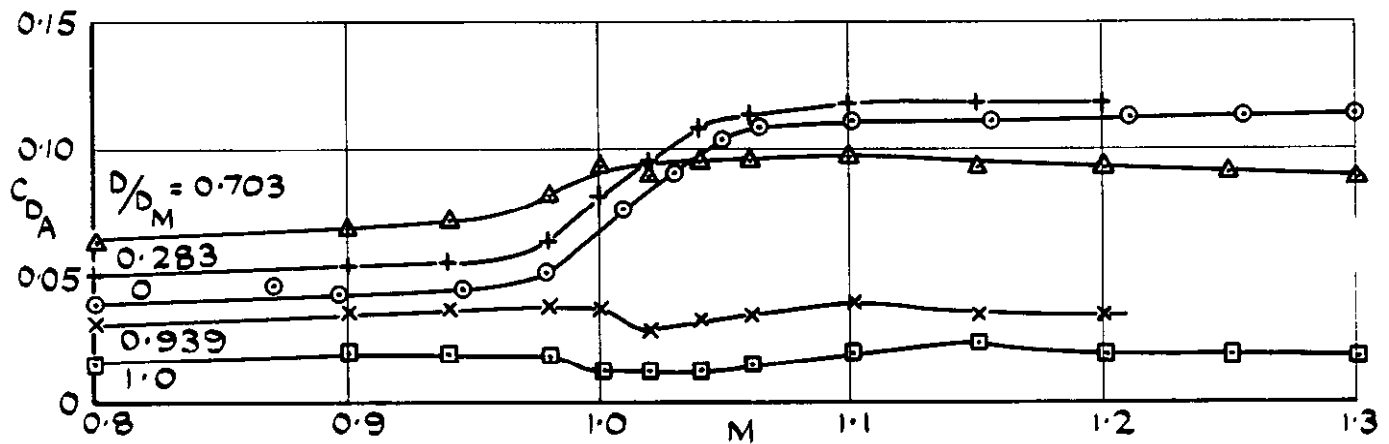
FIG. 9(b) AFTERBODY DRAG COEFFICIENT
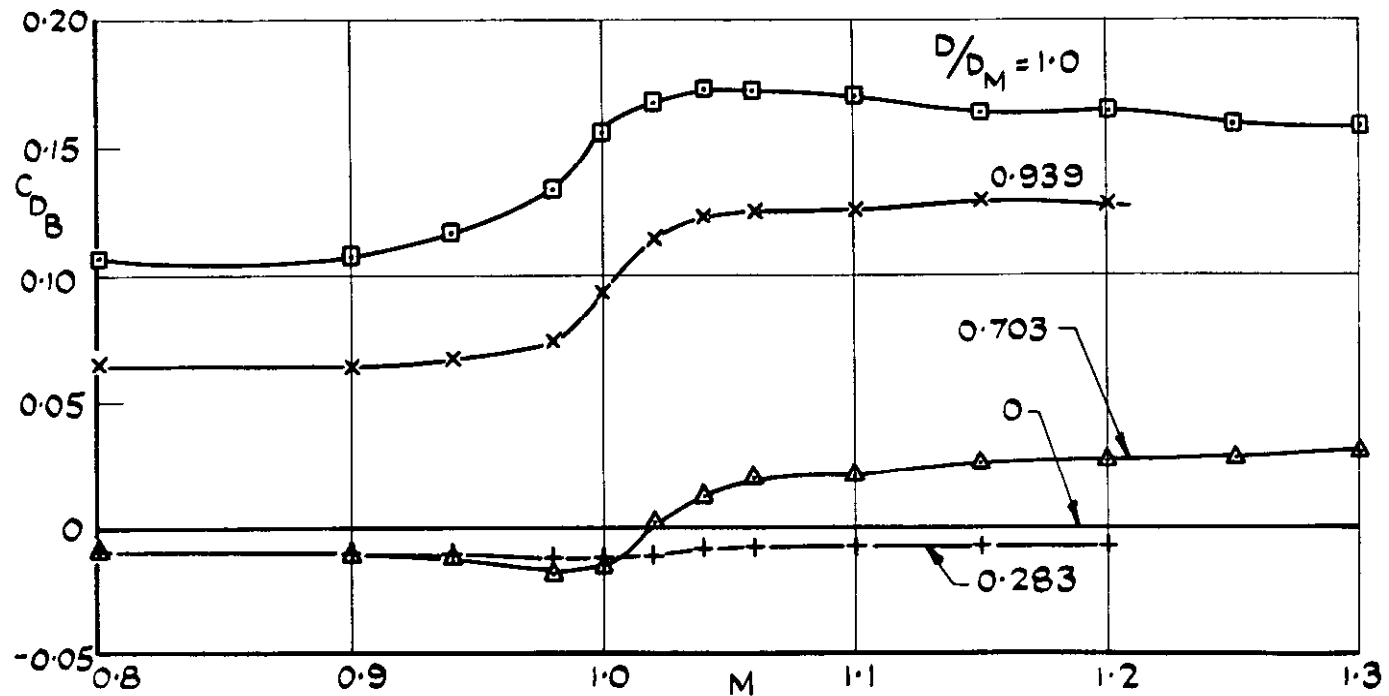
FIG. 9(c) BASE DRAG COEFFICIENT

FIG. 9 VARIATION IN TOTAL AND COMPONENT DRAG
COEFFICIENTS WITH MACH NUMBER
FOR THE BODIES ALONE
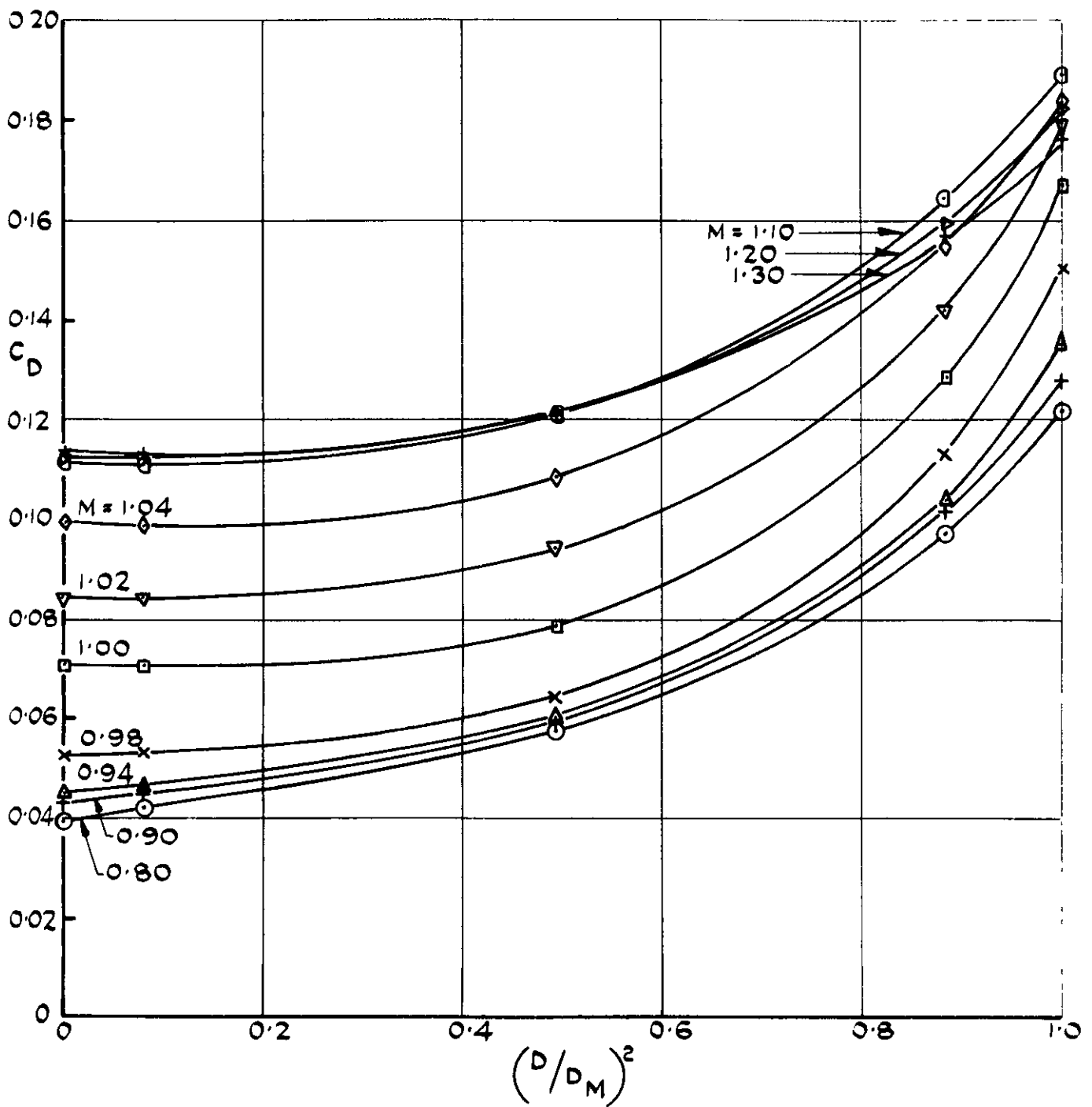
FIG.10(a) VARIATION OF TOTAL DRAG COEFFICIENT WITH BASE AREA (NO STING)
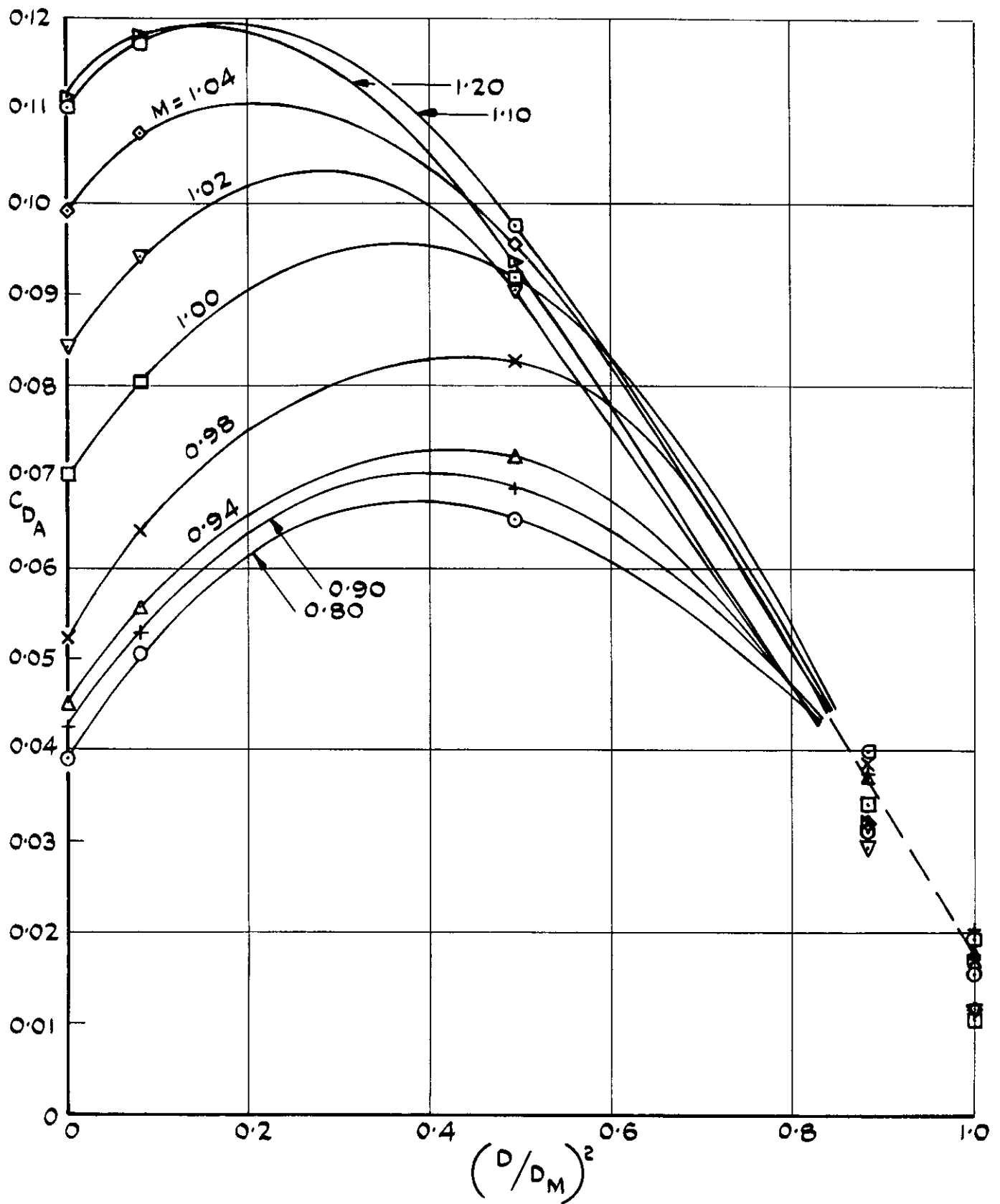
FIG. 10 (b) VARIATION OF AFTERBODY DRAG
COEFFICIENT WITH BASE AREA (NO STING)
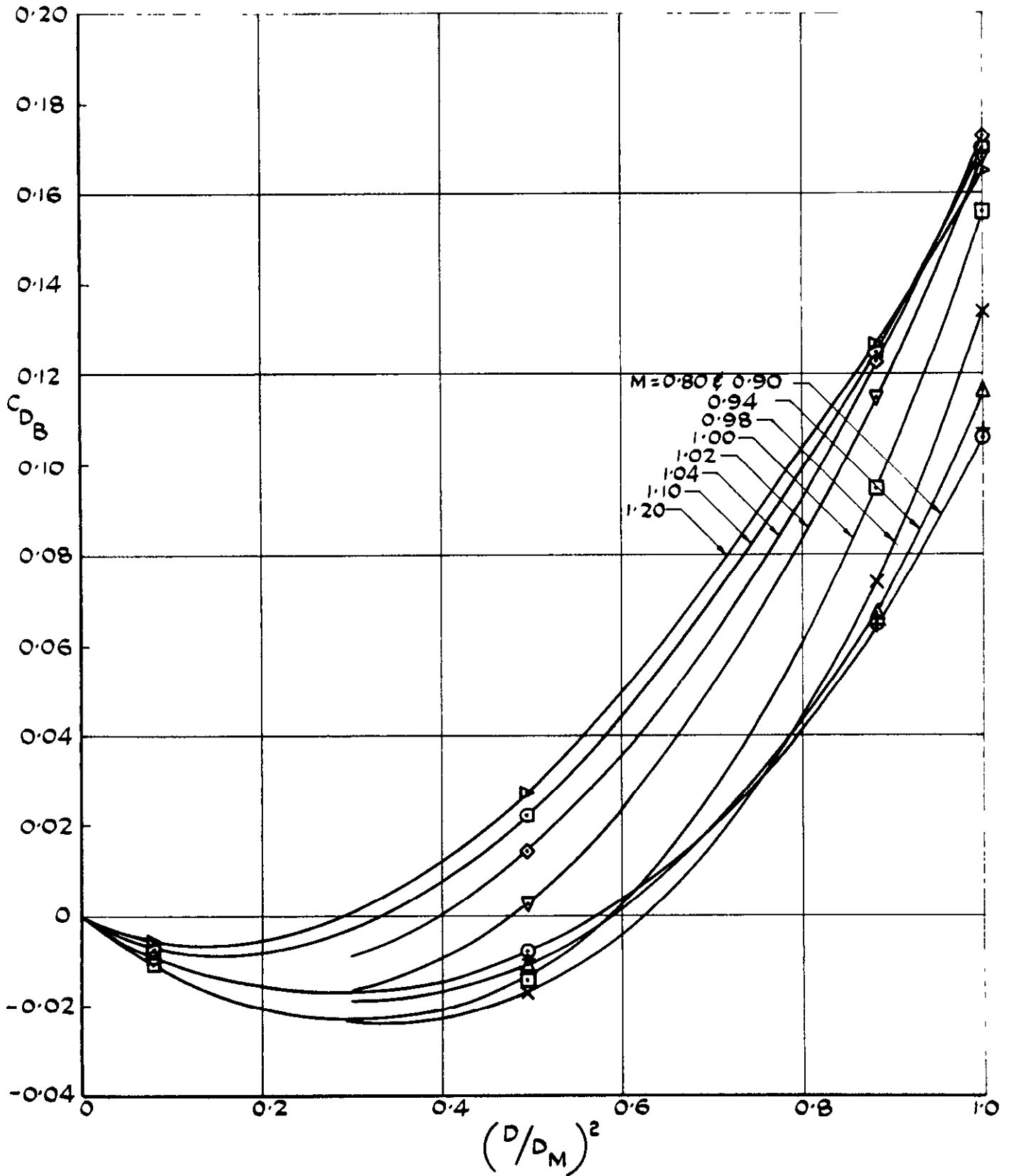
FIG·10 (c) VARIATION OF BASE DRAG
COEFFICIENT WITH BASE AREA (NO STING)
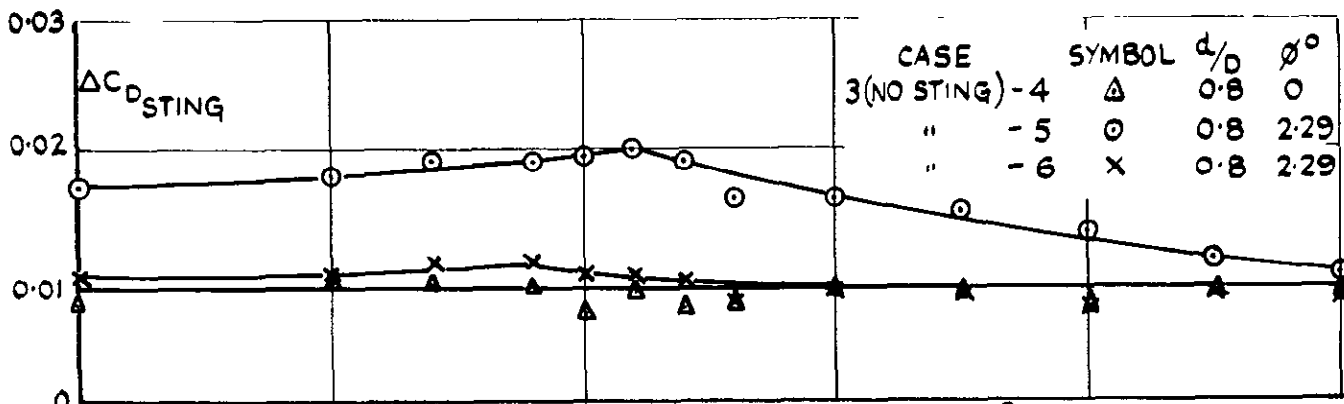
FIG. 11 (a) $D/D_M = 0.283$: $\beta = 14.6°$
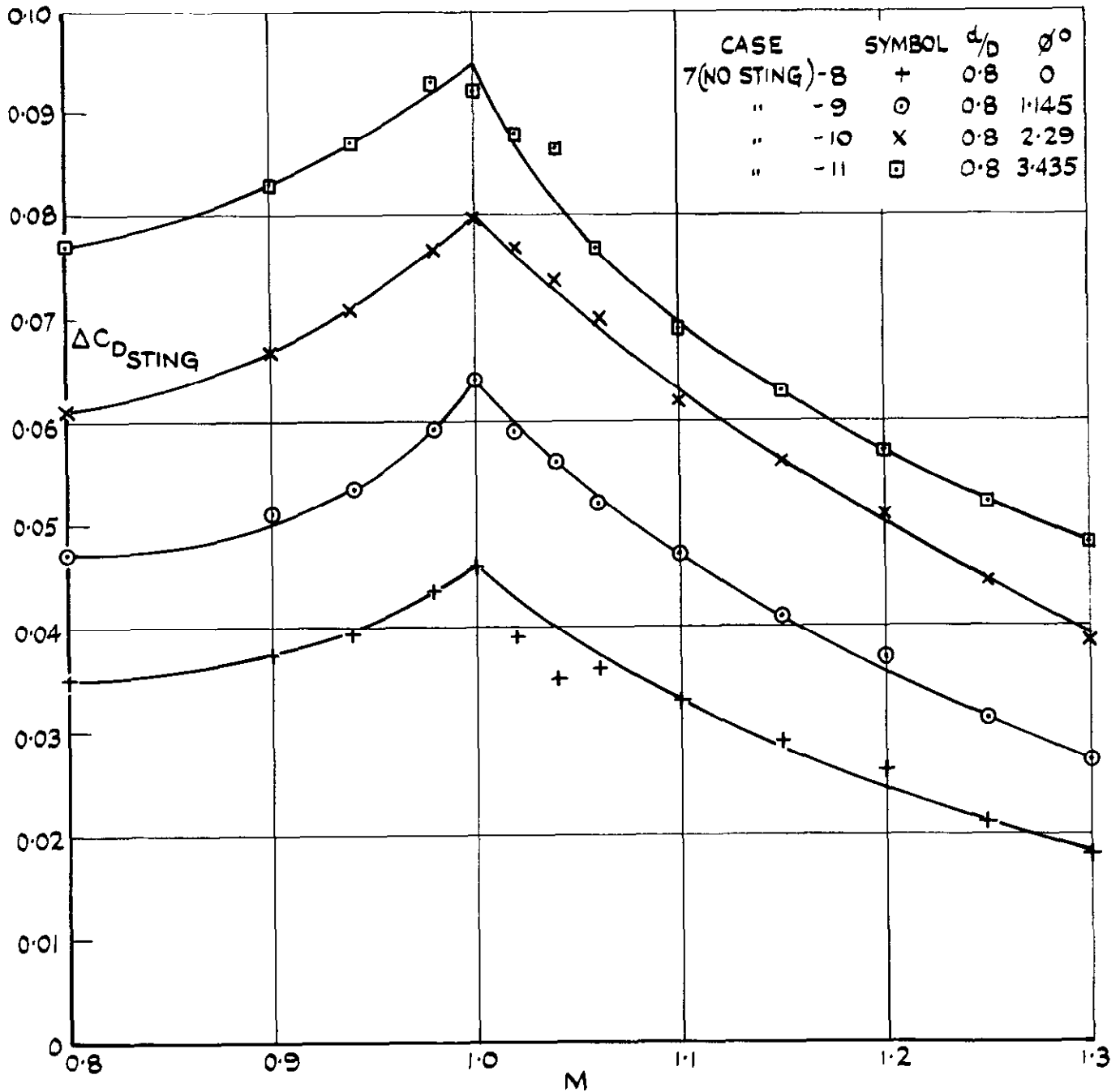
FIG. 11 (b) $D/D_M = 0.703$, $\beta = 9.6°$

FIG. 11 THE EFFECT ON THE DRAG OF VARIOUS
STING-BODY COMBINATIONS WHEN THE STING IS REMOVED
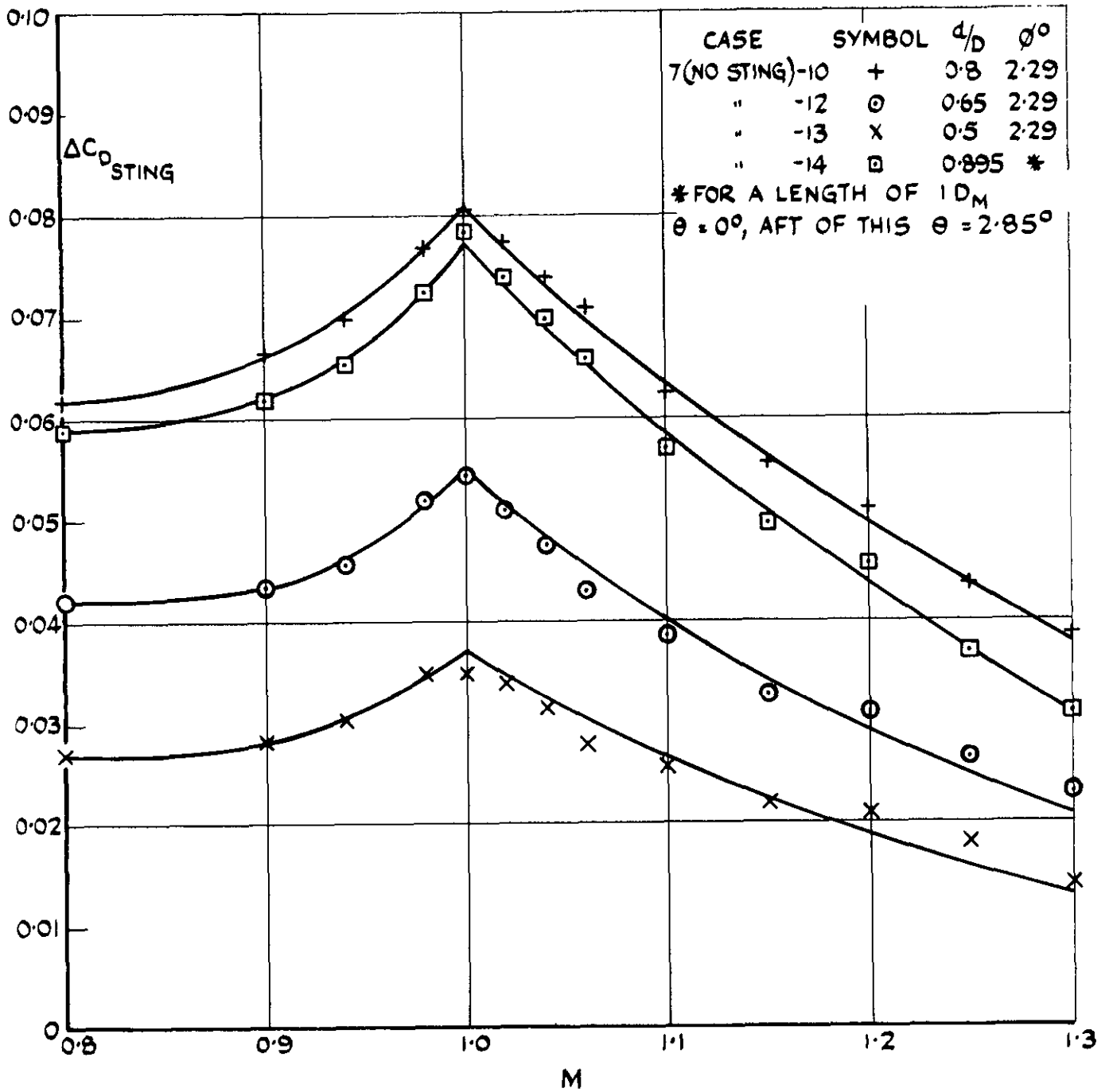
FIG. 11(b)(CONCLD) THE EFFECT ON THE DRAG OF VARIOUS STING-BODY
COMBINATIONS WHEN THE STING IS REMOVED $D/D_M = 0.703$, $\beta = 9.6°$
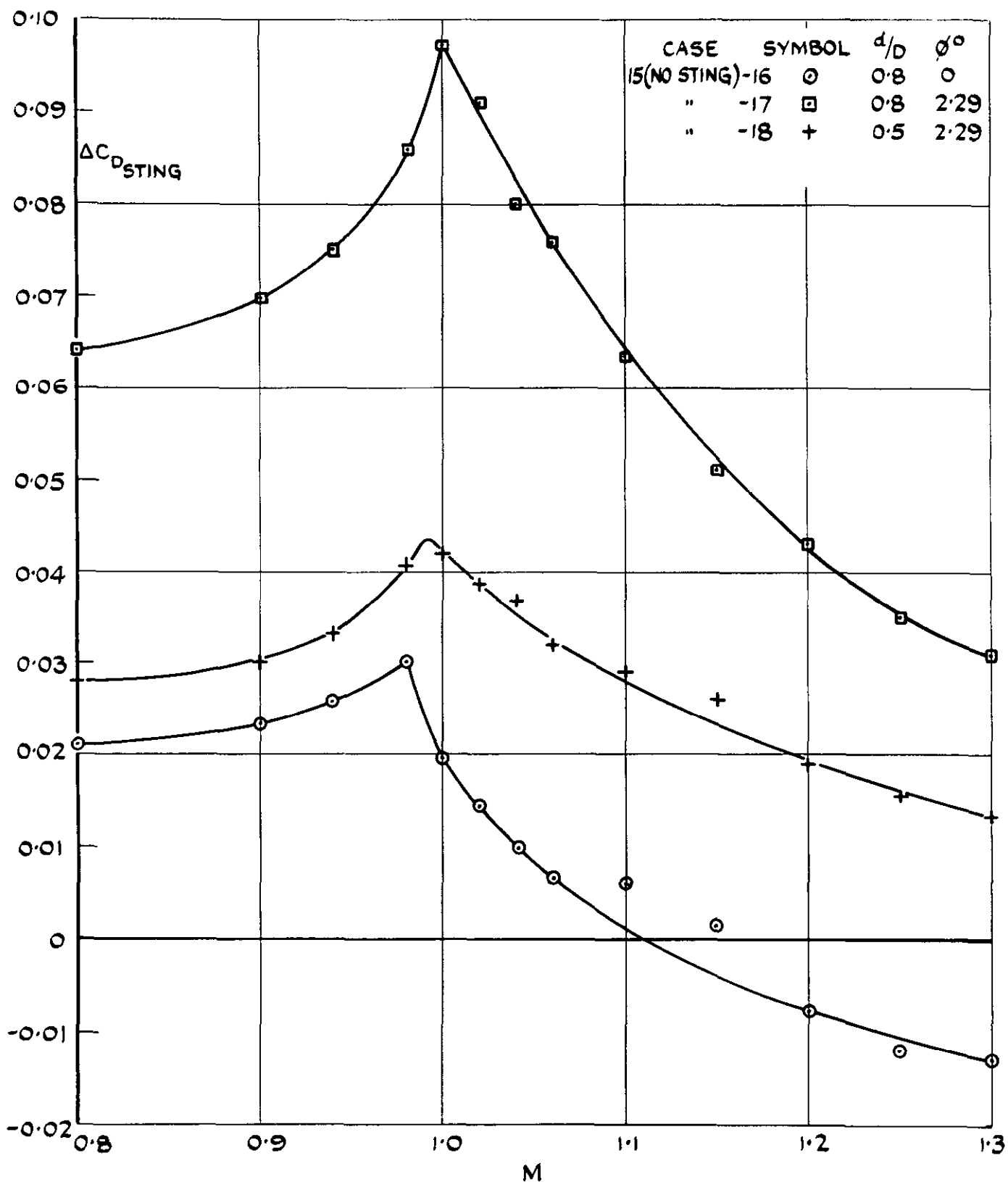
FIG 11 (c) THE EFFECT ON THE DRAG OF VARIOUS STING-BODY COMBINATIONS WHEN THE STING IS REMOVED $D/D_M = 0.939$, $\beta = 4.4°$
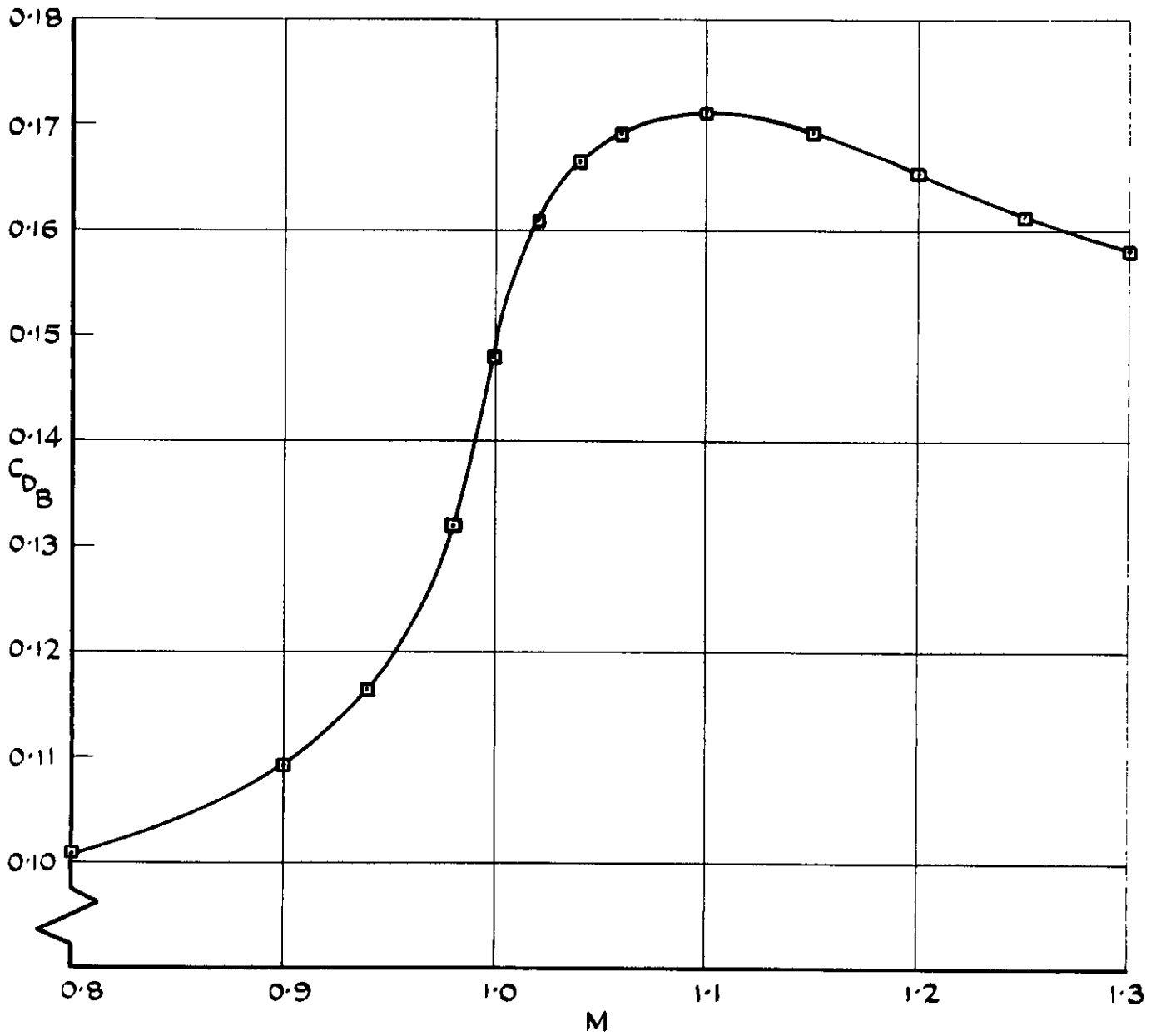
FIG. 12   BASE DRAG OF THE CYLINDRICAL MODEL
WITHOUT A STING
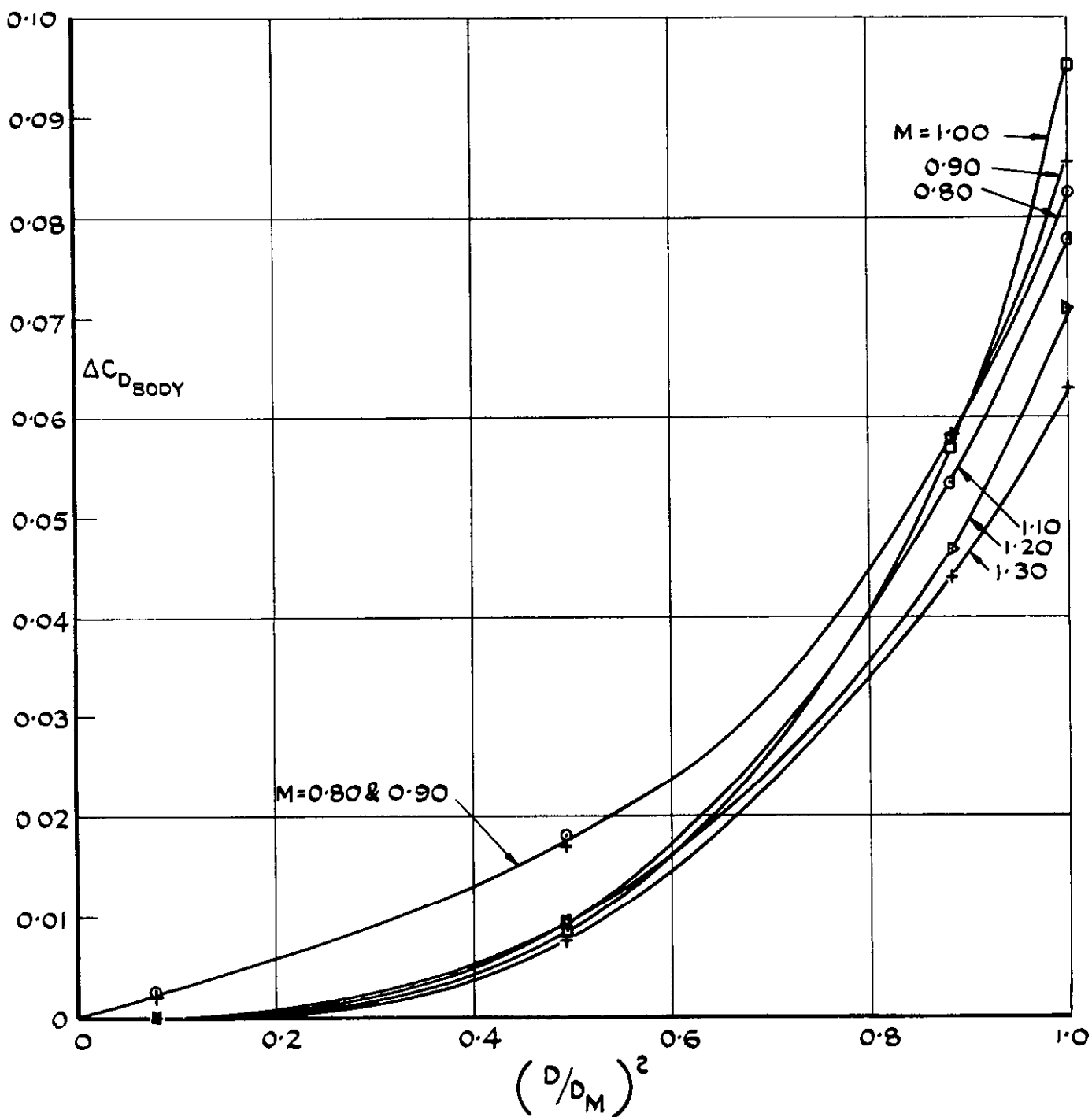
FIG.13   THE EFFECT ON DRAG OF SHORTENING
THE AFTERBODY (NO STING)
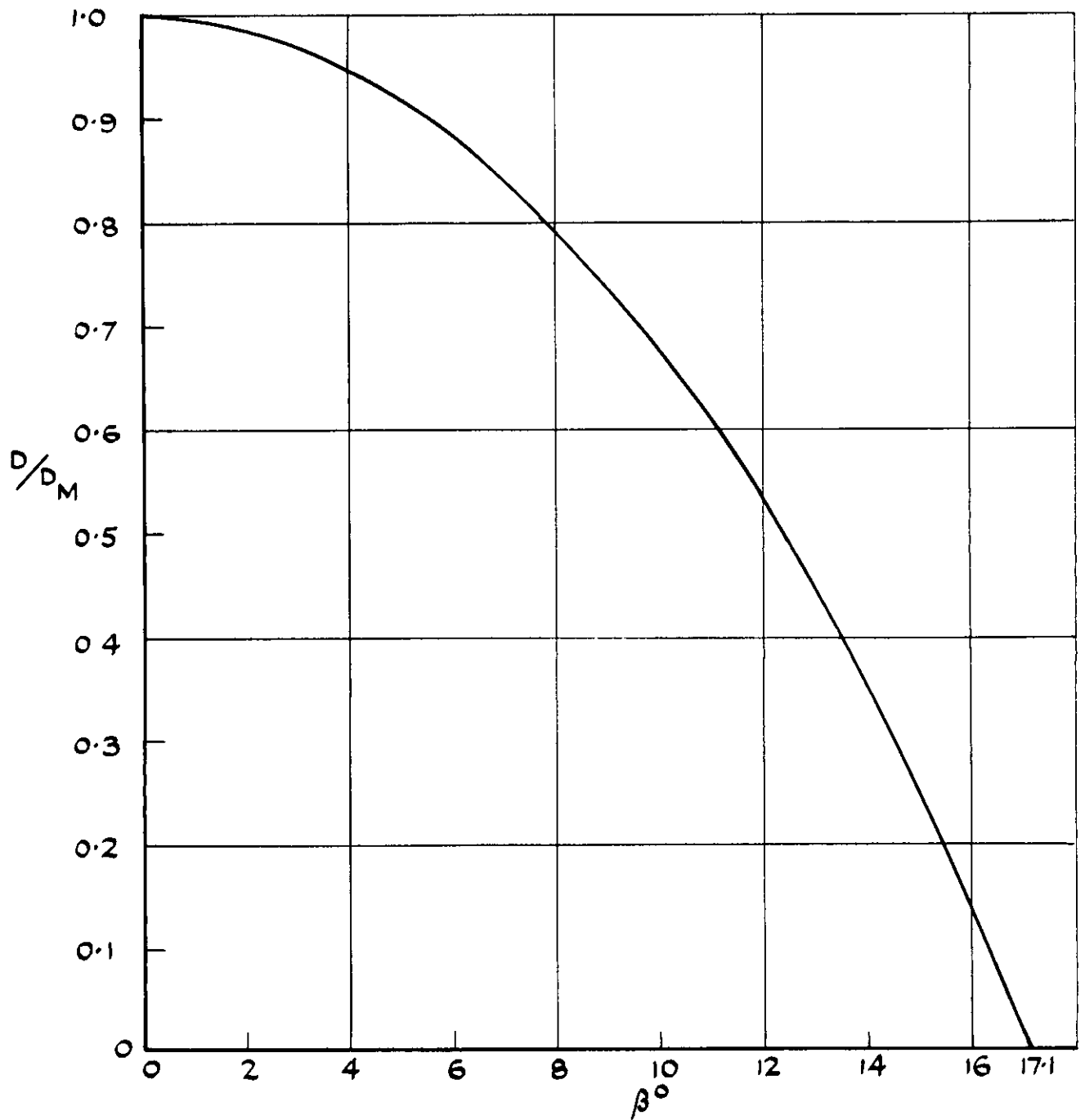
FIG. 14   BASE DIAMETER RELATED TO AFTERBODY

ANGLE AT THE BASE

A.R.C. C.P. No.984
September 1966

Kurn, A.G.

DRAG MEASUREMENTS ON A SERIES OF AFTERBODIES AT
TRANSONIC SPEEDS SHOWING THE EFFECT OF STING
INTERFERENCE

533.6.015.12 :
533.696.8 :
533.6.071.32 :
533.6.071.4 :
533.6.011.35

A number of axi-symmetric afterbodies consisting of the basic profile, a
tangent ogive with a fineness ratio of 3.33, and progressively truncated
versions of this shape were tested at zero incidence over a Mach number
range from 0.8 to 1.3. Measurements were made of the afterbody pressure
distribution, the base pressure and the total drag with and without the
presence of various rear stings.

In general the drag, in the absence of a sting, was increased by truncating
the ogive, but at supersonic speeds small truncations had little effect.

(Over)

The results at a given free stream Mach number show that, for the different stings fitted to each afterbody, there is an approximately linear relationship between afterbody drag and base pressure. Curves are presented whereby the measured total drag of the sting-mounted afterbody model may be corrected to obtain the true total drag in the absence of the sting.

The results at a given free stream Mach number show that, for the different stings fitted to each afterbody, there is an approximately linear relationship between afterbody drag and base pressure. Curves are presented whereby the measured total drag of the sting-mounted afterbody model may be corrected to obtain the true total drag in the absence of the sting.

The results at a given free stream Mach number show that, for the different stings fitted to each afterbody, there is an approximately linear relationship between afterbody drag and base pressure. Curves are presented whereby the measured total drag of the sting-mounted afterbody model may be corrected to obtain the true total drag in the absence of the sting.